

Provably Valid and Diverse Mutations of Real-World Media Data for DNN Testing

Yuanyuan Yuan, Qi Pang, Shuai Wang *Member, IEEE*,
The Hong Kong University of Science and Technology
{yyuanaq, qpangaa, shuaiw}@cse.ust.hk

Abstract—Deep neural networks (DNNs) often accept high-dimensional media data (e.g., photos, text, and audio) and understand their perceptual content (e.g., a cat). To test DNNs, *diverse* inputs are needed to trigger mis-predictions. Some preliminary works use byte-level mutations or domain-specific filters (e.g., foggy), whose enabled mutations may be limited and likely error-prone. State-of-the-art (SOTA) works employ deep generative models to generate (infinite) inputs. Also, to keep the mutated inputs perceptually *valid* (e.g., a cat remains a “cat” after mutation), existing efforts rely on imprecise and less generalizable heuristics. This study revisits two key objectives in media input mutation — perception diversity (DIV) and validity (VAL) — in a rigorous manner based on manifold, a well-developed theory capturing perceptions of high-dimensional media data in a low-dimensional space. We show important results that DIV and VAL inextricably bound each other, and prove that SOTA generative model-based methods fundamentally fail to mutate *real-world media data* (either sacrificing DIV or VAL). In contrast, we discuss the feasibility of mutating real-world media data with provably high DIV and VAL based on manifold. Following, we concretize the technical solution of mutating media data of various formats (images, audios, text) via a *unified* manner based on manifold. Specifically, when media data are projected into a low-dimensional manifold, the data can be mutated by walking on the manifold with certain directions and step sizes. When contrasted with the input data, the mutated data exhibit encouraging DIV in the perceptual traits (e.g., lying vs. standing dog) while retaining reasonably high VAL (i.e., a dog remains a dog). We implement our techniques in DEEPWALK for testing DNNs. DEEPWALK constructs manifolds for media data offline. In online testing, DEEPWALK walks on manifolds to generate mutated media data with provably high DIV and VAL. Our evaluation tests DNNs executing various tasks (e.g., classification, self-driving, machine translation) and media data of different types (image, audio, text). DEEPWALK outperforms prior methods in terms of the testing comprehensiveness and can find more error-triggering inputs with higher quality. The tested DNNs, after repaired using DEEPWALK’s findings, exhibit better accuracy.

Index Terms—Deep learning testing, deep neural networks, metamorphic testing



1 INTRODUCTION

DEEP neural networks (DNNs) primarily process high-dimensional media data, such as image/text/audio, with perceptually meaningful contents (e.g., a dog) that are human-perceivable. It is widely accepted that DNNs make decisions based on perceptual contents in media inputs. Despite their rapid advancement and use in safety-critical scenarios, DNNs, like traditional software, can make incorrect predictions with fatal consequences.

To test DNNs, we often need to launch massive media input mutations to trigger DNN prediction errors. In this regard, it imposes a key demand on the perception *diversity* and perception *validity* of mutated media inputs. Media inputs are desirable to be diverse, thus better stressing the DNN and exposing its faults. Moreover, media inputs are well-formed (e.g., RGB image pixels range from [0, 255]) and contain perception-level constraints. DNN faults triggered by ill-formed inputs or inputs with broken perceptions are less useful, as they are not specifically considered by DNNs. Note that DNNs do not feature “input check,” and they generally assume that test inputs are correlated with training inputs, and both test and training inputs are real-world meaningful media data.

Existing research has tested DNNs by randomly changing their input data bytes (e.g., adding random noise to images) [2]. These methods mutate only limited bytes per input, hardly affecting the visual diversity or may generate inputs with broken content. Recent works use weather filters or knowledge transfer techniques [3], [4] to mutate media data. However, they are limited to specific scenarios or data types like traffic scene images [5], [6], [7], [8] or natural language text [9], [10], [11], [12]. Even worse, to generate perceptually valid image/text, existing works rely on heuristics or domain-specific checks [13], [4], such as bounding the maximal number of mutated pixels. These validation methods are often less generalizable and heavily rely on pre-trained oracle models. Worse, they may overlook format-invalid data; as shown in Sec. 7.

The state-of-the-art (SOTA) works, [14] and [15] characterize all images via a unified latent space, and they generate media data using advanced deep generative models. With generative models, they can generate unlimited and diverse media data as the test inputs of DNNs. However, this paper demonstrates, via both rigorous proof and empirical evaluation, that SOTA works are *only* applicable to toy datasets like MNIST [16] (i.e., images of handwritten digits).

This work aims to enhance media data mutation, a key step in DNN testing. Despite having been widely discussed in existing literatures, this task is yet rigorously formulated,

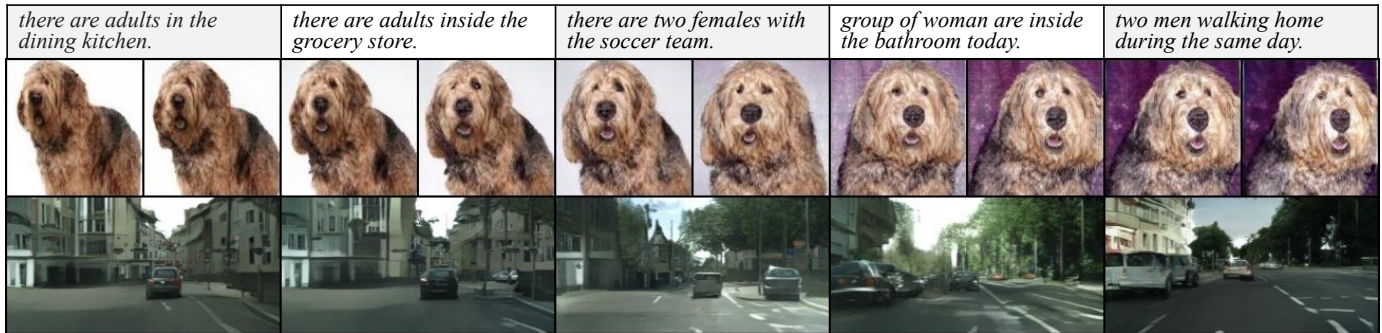


Fig. 1. Perceptual-level mutations of DEEPWALK by walking towards one direction with a fixed step size on manifolds. DEEPWALK can mutate images, audio, and natural language text; see [1] for more cases.

leading to less practical or spurious methods. Therefore, we focus on the two key objectives: *perception diversity* (DIV) and *perception validity* (VAL). We formulate DIV and VAL quantitatively based on manifold, a well-established concept in representation learning, that encapsulates perceptions of high-dimensional media data in low-dimensional spaces [17], [18]. Then, we discover important and inextricable constraints between DIV and VAL: VAL is bounded by DIV, and when images in different manifolds are mapped to one latent space (as in SOTA works [14], [15]), the bound is *provably negligible*, greatly impeding mutating media data while retaining a reasonable VAL. This way, we respectfully rebut SOTA works by proving that they inevitably sacrifice VAL when mutating *real-world media data*. In contrast, we show the feasibility of mutating real-world media data with provably high DIV and VAL on the basis of manifold.

Concretely, we propose the technical approach of mutating media data by “walking” on their manifolds, enabling format-agnostic mutations toward image/audio/text without domain knowledge. As in Fig. 1, media data can be mutated by first projecting them into respective manifolds, and then moving them along the manifold in specific directions and step sizes. Contrasted with the original data, the mutated data exhibit diverse changes in the perceptual traits (e.g., left-oriented vs. right-oriented face). It also retains the perceptual-level validity (e.g., a dog is still a dog).

We implement DEEPWALK, an efficient and practical DNN testing framework. DEEPWALK constructs a set of manifolds \mathbb{M} for media data in an *offline* phase. Then, DEEPWALK launches an *online* testing phase, where it walks on each $\mathcal{M} \subset \mathbb{M}$ in various directions and step sizes, under the feedback of standard DNN testing objectives such as structural coverage [2], distribution-wise coverage [19], cluster-based coverage [5], or black-box objective. The coordinates covered on the manifold are mapped back to high-dimensional space. Thus, media data with diverse but nevertheless valid perceptions can be used to test DNNs and reveal their prediction inconsistencies.

Nineteen popular DNNs that analyze media data in image, audio, and text formats are evaluated. The working contexts range from generic (e.g., image classification) to specific (e.g., autonomous driving). We compared DEEPWALK with previous generative model-based methods (e.g., DeepRoad [4]), and four de facto feedback-driven testing frameworks — DeepHunter [13], TensorFuzz [5], DeepS-

mart [20], and DeepTest [3]. DEEPWALK has considerably better performance than the previous works in 92 out of 95 quantitative evaluations. In comparison with all previous works, DEEPWALK also demonstrates promising results by recognizing more and diverse error-triggering inputs. Media data mutated by DEEPWALK are of better quality and can be used to better repair DNNs, outperforming previous works. By mutating image, text, and audio inputs, we demonstrate the versatility of DEEPWALK in testing DNNs for image classification, autonomous driving, machine translation, and audio classification. Ablation studies also prove the superiority of DEEPWALK’s design considerations. In sum, this work makes the following major contributions:

- We rigorously formulate two key objectives of input mutations in DNN testing, perception diversity (DIV) and validity (VAL), based on manifold. We prove important results that DIV and VAL inextricably bound each other, and respectfully rebut SOTA works by proving their incapability in front of real-world media data.
- Following, we propose practically feasible solutions to mutate media data with provably high DIV and VAL based on manifold. We concretize this design by first recasting media data into manifolds and then performing perceptual-level mutations.
- We implement DEEPWALK to allow mutating media data of several formats without any domain knowledge or templates. DEEPWALK incorporates design principles and optimizations to explore perception changes that can trigger DNN faults under feedback of off-the-shelf DNN testing objectives.
- We evaluate DEEPWALK using real-world DNNs that process images, audio, and text. We show that media data with provably high DIV and VAL are produced, and that DEEPWALK achieves good performance w.r.t. various criteria and significantly outperforms all previous frameworks.

Full code and data of DEEPWALK are provided at the website [1]. We will maintain DEEPWALK to benefit follow-up research comparison and usage.

2 PRELIMINARIES AND MOTIVATION

In this section, we briefly review how different DNNs process perceptions. We then show key properties of media data and introduce the concept of data manifold.

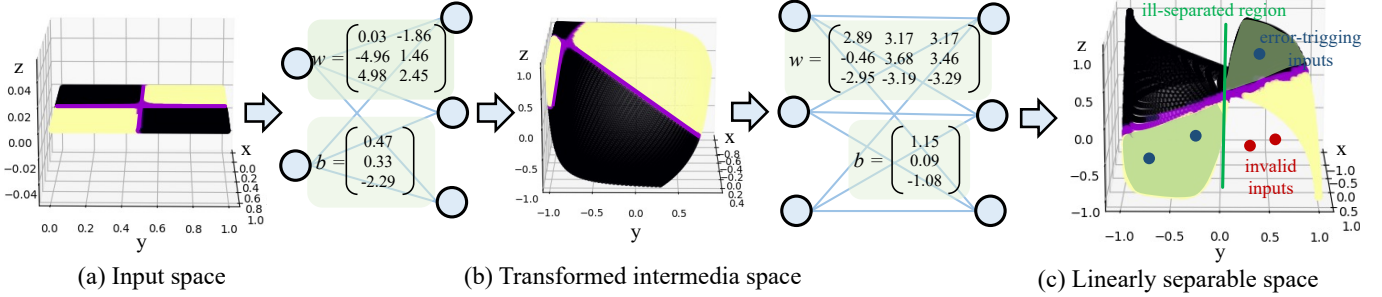


Fig. 2. A two-layer DNN that solves the XOR problem and predicts outputs for $(x > 0.5) \oplus (y > 0.5)$. The input space from (a) is progressively transformed as linearly separable in (c). In (b) and (c), each dimension (i.e., x , y and z) denotes one neuron and its outputs.

2.1 Deep Neural Network

Most DNNs can be categorized into feed-forward neural networks (FNNs) and recurrent neural networks (RNNs). We introduce how media data perceptions are extracted and processed by them.

FNNs. A Convolutional Neural Network (CNN) denotes one representative FNN. In general, a CNN is trained to focus on the essential perceptual content of images, which may include object types, colors, and motions. Its training is mainly accomplished by using the convolutional kernel, which simulates how humans spot and recognize patterns in images, regardless of the angle from which the images are seen. FNNs are widely used in image understanding, e.g., classification, where perceptual content is retrieved for coarse-grained labeling. Further, perceptual features are extensively tagged with, for example, driver decision or disease information to facilitate domain-specific activities such as self-driving and disease diagnostics. *Translation invariance* is a crucial characteristic enforced by a CNN, which means that perceptual items (e.g., a cat) may be recognized in an image even if their appearance changes [21]. This characteristic improves a CNN’s ability to process a wide range of images in real-world circumstances. However, as discussed later in Sec. 7, translation invariance can hamper the efficiency of previous DNN testing methods that alter images using affine transformations [3]. In contrast, we will show that DEEPWALK delivers an effective and unified testing pipeline toward FNNs used in general image understanding and domain-specific tasks (auto-driving and audio processing) by mutating perceptions.

RNNs. Derived from FNNs, RNNs are capable of processing variable-length sequences, e.g., natural language sentences. For such data, a “sequence” usually contains more informative perceptions than individual elements do [22]. RNNs are often used for text comprehension, such as machine translation (MT), where word dependency in a language is captured by RNNs. Random mutation can easily damage discrete data like text; therefore, previous RNN testing relied heavily on predefined text-mutation templates [9], [10], [11], [12]. However, template-based approaches have a limited generality and are likely to miss faults in real-life corner cases. In contrast, DEEPWALK delivers perceptual-level mutation by walking on manifolds which characterize properties of the language. This enables a thorough exploration of the RNN input space while simultaneously ensuring the validity of mutated text.

DNN Faults. A DNN layer can be represented as $\text{Act}(W\mathbb{X} + b)$, with \mathbb{X} being the input space. (W, b) forms an affine¹ transformation over \mathbb{X} . The non-linear activate function Act bends \mathbb{X} to better split regions, e.g., $\text{ReLU} : y = \max(0, x)$ bends the straight line $y = x$ at $(0, 0)$ in a two-dimensional space. In Fig. 2, a sample neural network solves the XOR problem that is not linearly separable. The input space is $(x, y) \in [0, 1] \times [0, 1]$ and is labelled as $(x > 0.5) \oplus (y > 0.5)$. By progressively transforming the input space via each layer, inputs sharing similar properties are gathered.² Finally, the space is separated (using the purple line in Fig. 2(c)) as two linearly separable regions with different labels. Aligned with existing works, we characterize DNN faults in the following.

DNN faults root from the incorrect separation (i.e., wrong decision boundaries). Error-triggering inputs in the ill-separated regions have similar properties, which are typically referred to as DNN *biases*: DNN testing should be designed to detect such biases.

On the other hand, suppose most training data in Fig. 2(a) have $x < 0.5$. The DNN thus primarily relies on the value of y to predict the XOR output, resulting in **ill-separated regions** in Fig. 2(c). Error-triggering inputs (blue dots) in these ill-separated regions would have $x > 0.5$ when they are mapped back to Fig. 2(a). This shows that the faulty DNN has a bias on the value of x . From a holistic view, DEEPWALK can identify critical perception changes in real-world media data of different contents and types that expose *perception biases* of faulty DNNs.

DNN Inputs. Also, as shown in Fig. 2(c), the input space is largely twisted after transformations. Common DNN testing objectives, such as neuron coverage, aim at maximizing the covered output range of each neuron, which unavoidably induces invalid inputs (red dots in Fig. 2(c)) to test DNNs. Though in this demo, we can explicitly restrict inputs to $[0, 1] \times [0, 1]$ to rule out those invalid inputs, the constraints formed by perceptual contents over arbitrary real-world media data bytes are hard to obtain. We therefore point out the following difficulty of testing DNNs:

1. A geometric transformation that preserves lines and parallelism.
2. For high-dimensional media data like images, “inputs sharing similar properties” can be dog photos where every dog in the photo is consistently left-oriented.

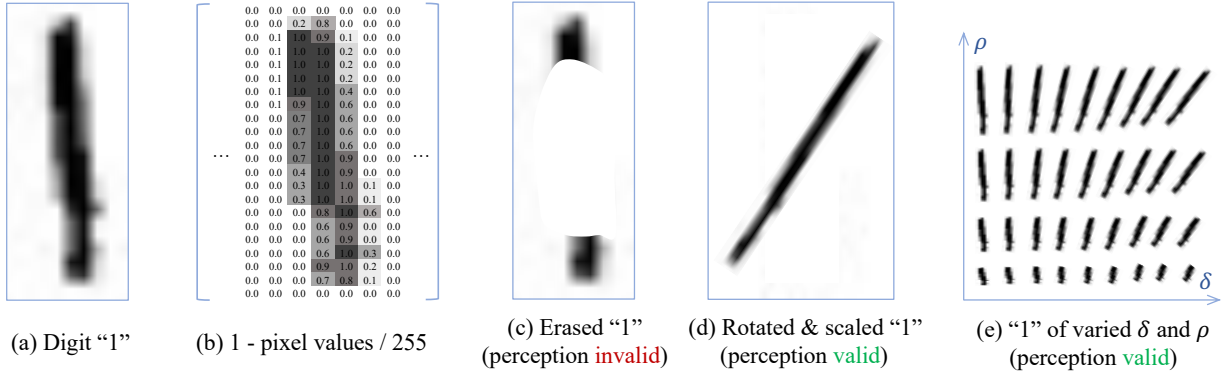


Fig. 3. Demonstration of key properties of media data using an image of digit “1”. As in (b), to form a valid digit “1”, there exist constrains over pixel values. Comparison between (c) and (d) illustrates the incapability of measuring VAL using pixel-based criteria. (e) simplifies each digit “1” as a segment and represents them with length ρ and rotation angle δ .

Given DNNs do not feature “input checks” and perceptual constraints over media data are not explicit, it’s demanding albeit challenging to ensure the validity of mutated media inputs.

Previous mutations can frequently break the perceptual contents in media data. Recent SOTA works [14], [15] can generate perceptually valid images by converting all images into a unified latent space via generative models. Nevertheless, as will be proved in Sec. 4, their schemes are inapplicable for real media data, where only meaningful data are produced.

2.2 Media Data and Manifold

We now elaborate on key properties of media data. Though using images as an example, mutating other media data suffers from similar challenges introduced in this section.

Fig. 3(a) shows a 28×28 image of digit “1” (with margins cropped) from the MNIST dataset, which has 784 dimensions in the pixel space. As shown in Fig. 3(b), pixel values share perceptual constraints to form a valid “1”: randomly sampling pixels from $[0, 255]$ mostly provides noise.

Pixel Space. The 784-dimensional pixel space for digit “1” is highly redundant, given only a small portion of data samples are valid “1”. Moreover, it is hard to measure/-validate mutations in this space. As shown in Fig. 3(c), when most parts of the digit are erased, the mutation breaks the perceptual contents. In contrast, Fig. 3(d) rotates and rescales the digit from Fig. 3(a), which still yields a valid “1”. Note that previous works often adopt pixel-wise distance criteria to decide the “validity” of mutated images, which is improper. For instance, though compared with Fig. 3(d), Fig. 3(c) has fewer pixels changed, it is improper to deem Fig. 3(c) as more realistic (perceptually valid).

Dimension Reduction. To ease the understanding, let’s simplify the digit “1” as a segment.³ Then, each digit “1” can be represented by length ρ and rotation angle δ in the polar coordinate, where the dimensions are largely reduced to two. Fig. 3(e) displays digits using ρ and δ . Obviously, it is easier to form a valid “1” by directly restricting the ranges of ρ and δ . And accordingly, it is also easier to produce

perceptually valid and diverse digits by changing ρ and δ within the constrained ranges.

Overall, to enable diverse and valid mutations for arbitrary high-dimensional media data in real-world settings, it is more desirable to explore a general and unified dimension reduction strategy for representing media data in a low-dimensional space that encodes perceptions. DEEPWALK fulfills the requirements by using data manifold. We now introduce manifold below.

Manifold. Perceptual contents in media data are captured via data manifold. Overall, manifold forms the basis of *manifold hypothesis*, which states that the high-dimensional space \mathcal{R} of real-world data embeds the manifold \mathcal{M} of much lower dimensions [23], [24]. For instance, let portrait photos concentrate to one manifold \mathcal{M}_p , \mathcal{M}_p shall retain constraints over certain pixels that jointly make up perceptions like head, ear and nose. Generally, manifolds preserve the “closeness” in perceptions of high-dimensional data. Also, data of the same class lie in one continuous manifold, whereas data of distinct classes (e.g., car vs. cat) lie in *disconnected* manifolds [23], [24]. Manifolds are typically adopted for dimensionality reduction, e.g., for PCA [25], where the principal components of each data point x should uniquely locate its projection on \mathcal{M} [17].

Manifold Construction. Manifolds used for PCA are constructed via linear functions. Nevertheless, linear approaches are not expressive since most real-world mappings between \mathcal{M} and \mathcal{R} are non-linear. Several non-linear methods are thus proposed [26], [27], [28]. These approaches are non-parametric, which only enable low-dimensional representations and are incapable of inferring other data points lying on \mathcal{M} . This work relies on manifold to mutate media data of different types in a provably diverse (DIV) and valid (VAL) manner for DNN testing. Enabled by recent advances in generative models [29], we construct projections $f_\theta : \mathcal{R} \rightarrow \mathcal{M}$ using *parametric* and *non-linear* approach, i.e., carefully crafted generative models (which are different from those in SOTA works; see details in Sec. 5).

Image Manifold. Fig. 4 depicts the variety of Border Collie photos on a manifold \mathcal{M} . Using DEEPWALK, we project a set of Border Collie photos into coordinate z on \mathcal{M} of 120 dimensions. To ease the presentation, we further pick the first two z -values, d_1 and d_2 , to form a 2D manifold on Fig. 4.

3. A digit “1” is more complicated than a segment, but the required extra dimensions should not be too many.

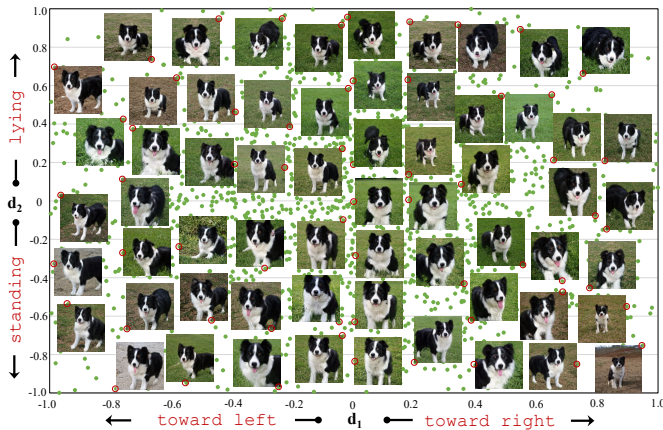


Fig. 4. Visualization of the manifold (constructed by DEEPWALK) of Border Collie photos, where Border Collies sharing similar properties are gathered (e.g., left-oriented when $d_1 < 0$).

We then pick coordinates on Fig. 4, marked in red cycles, and use DEEPWALK to map them to images. Despite its two-dimensionality, the visualization in Fig. 4 is informative to clarify the concept of manifold. The hue of the background grass gathers images. Also, most Collies stand when $d_2 < 0$ and lie down if $d_2 > 0$ (particularly when $d_1 = 0$). The value of d_1 seems to be related with the orientation since most of the Collies look left when $d_1 < 0$, and vice versa.

Text/Audio Manifold. Manifolds of text data constrain primarily the word dependencies, which further encode the semantics and grammatical coherence of sentences [30], [31]. For instance, mutating sentences in \mathcal{M} can modify the subjects or change the described events (see Fig. 1). Similarly, audio manifolds may enclose the spoken words and tones [32], [33], allowing for changes in intonation when mutating audios via manifolds.

We clarify that manifold is more *comprehensive* than training data. For Fig. 4, if we only have images whose projected d_1 and d_2 have the same sign, i.e., $\langle \text{lying, toward right} \rangle$ Collies and $\langle \text{standing, toward left} \rangle$ Collies, by inferring perceptual-level changes from these images, manifold \mathcal{R} in Fig. 4 can still be created and enables the construction of $\langle \text{lying, toward left} \rangle$ Collies and $\langle \text{standing, toward right} \rangle$ Collies. This reveals the feasibility to launch full-fledged DNN testing by systematically exploring manifolds.

Walking on a Manifold. Performing perceptual-level mutations over media data involves two orthogonal aspects, namely, mutating which perceptions and to what extent a perception is mutated. These two aspects can be characterized as the *walking direction* and the *step size* on a manifold. Suppose the training data corresponding to Fig. 4 is biased to standing Collies such that the trained DNN incorrectly relies on “standing” to classify an image as Collies. DEEPWALK, by walking upwards with a large step size, mutates Collies to be lying down, effectively stressing DNNs and likely triggering mis-classifications. We present several examples of perceptual-level sentence/image mutation in Fig. 1. The mutation is performed when DEEPWALK walks towards one direction on the manifold and each sentence/image denotes one footprint of DEEPWALK.

3 RELATED WORK

We review existing works in generating diverse (DIV) media data in Sec. 3.1 and Sec. 3.3. We then review methods to preserve format and perception validity (VAL) of mutated media data in Sec. 3.2.

3.1 Producing Diverse Media Data with Mutation

Fig. 5 compares image mutation launched by existing methods and by DEEPWALK. We summarize the application of existing mutation methods to images and discuss their extension to text:

Pixel-Level Transformation changes image brightness or contrast, or adds noise. DeepXplore [2] uses pixel-wise mutations in a whitebox context under the guidance of target DNN’s gradients. It comprises two schemes: randomly adding black blocks or perturbing user-specified regions with noise generated from gradients. Pixel-level mutations can be ineffective as images usually have many pixels. Both approaches may damage the image VAL, and even violate labels of original images (e.g., tearing objects in a photo).

Affine Transformations translate/rotate/scale/shear an image while preserving the collinearity after mutation (see Fig. 5(a)). As discussed in Sec. 2.1, the *translation invariance* of a CNN may hinder affine transformations.

Convolutional Transformations perform holistic modification of an image, such as blurring or adding domain-specific (e.g., rainy) filters.

Affine and convolutional transformations are first considered in DeepTest [3]. DeepSmart [20] divides an image into sections and mutates one at a time. Modifying only one section may result in fragmented images. Overall, despite affine/convolutional transformations offer more holistic mutations, these changes are usually limited and require domain knowledge (e.g., a traffic scene should be rotated by a small angle). Thus, the “behaviors” of target DNNs are often not fully tested.

Knowledge Transfer transforms data from one domain to another by leveraging knowledge from the target domain. DeepRoad [4] and TACTIC [34] mutate images using *style transfer* techniques [35], [36]. Their strength (and limits) stems from *cycle-consistency* training [35], a popular learning paradigm for generative models. For example, given street images taken on sunny and snowy days, these techniques enhance sunny-street images by gradually changing the weather to snowy, and vice versa. Weather conditions provided by “cycle-consistency” are more realistic than those added by convolutional transformations and are not confined to a few available templates. However, the availability of photos from two domains limits this strategy (e.g., photos taken from two weather conditions are needed). “Knowledge transfer” also fails when images in two domains have significant geometric distinctions [37]. This method has only been used to test autonomous driving [4]. It is difficult to extend the method to arbitrary real-life scenarios.

Text. Existing works heavily study mutating images. However, real-world DNN models analyze various types of media data, such as text. A “pixel-level” mutation similar to that for images is impractical in the case of text because random perturbation of words will not retain grammatical or linguistic coherence. Most text mutations are performed using pre-defined templates or heuristics [9], [10], [11], [12].

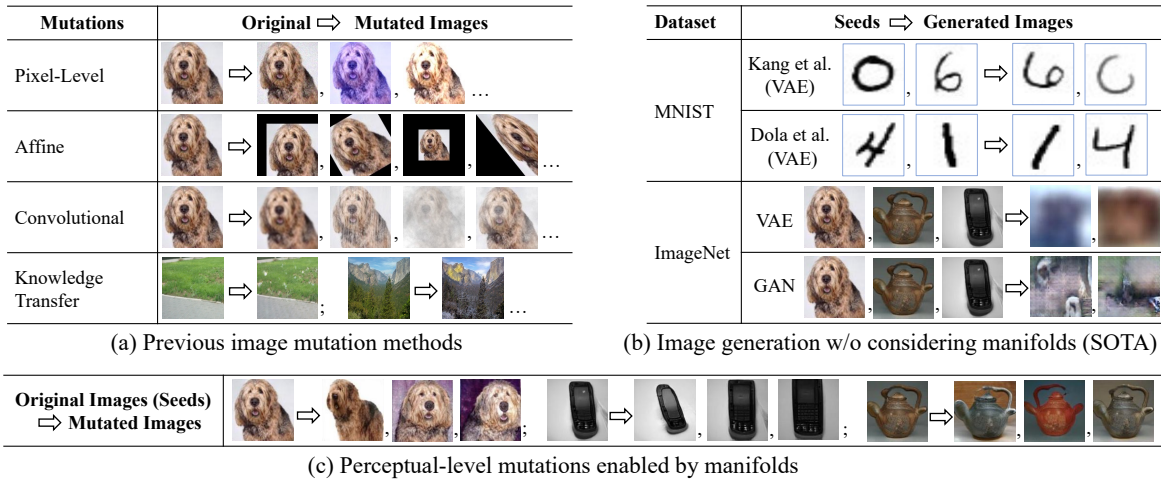


Fig. 5. Illustration of previous (a) image mutations and (b) image generation w/o consider manifolds. (c) shows the perceptual-level mutations of DEEPWALK enabled by data manifold.

3.2 Ensuring Format and Perception Validity of Mutated Media Data

On top of the restrictions defined by formats (e.g., RGB images’ pixel values must in $[0, 255]$), the VAL of media data requires perceptual contents being retained after mutations (e.g., a cat is still a “cat”). To clarify, VAL is often referred to as *realism* of mutated media data by previous works [13], [3], [4]. Mutations introduced in Sec. 3.1 can generate unrealistic data, and therefore, extra validation procedures are performed by existing works. A grammatical check can validate natural language sentences. However, validating mutated images is more difficult and often involves heuristics.

TensorFuzz [5] adds pixel-wise noise to images. It enforces the realism of mutated images by truncating accumulated noise to a user-defined range. DeepTest [3] limits the parameters of each transformation to a specific range. DeepTest also assesses mean squared error (MSE) to rule out likely broken images. However, as found in Sec. 7.1, many of its mutated images, though passed its validation, are barely identifiable to humans. DeepHunter [13] allows only one-time affine transformation on each image. It uses thresholds to bound #mutated pixels and mutated pixel values for pixel-level transformations. However, as discussed in Sec. 2.2, pixel-based criteria can hardly ensure VAL, let alone the criteria itself is sensitive to thresholds. DeepRoad [4] ensures authenticity by rejecting an image with features that are significantly different from features in training data. The features are extracted by a pre-trained oracle model (VGG [38]). It also assumes the availability of the target DNN’s training dataset, which may not be available.

Moreover, as shown in Sec. 7.1, since pixel-level mutations directly change pixel values, existing validation schemes can neglect images of invalid format (e.g., pixel values outside $[0, 255]$) if the format restriction is not explicitly considered. They also frequently overlook images of broken perceptions. DEEPWALK only mutates perceptions and always produces format-valid media data (as it never directly alters pixel values). The perceptual contents are also meaningful under the constraints formed by data manifold; see Sec. 4.3 for details.

3.3 Generating Diverse & Valid Images Using Toy Datasets with Generative Models

Recent works [14], [15], [39], [40], [41], including SOTA works [14], [15], use generative models like generative adversarial network (GAN) [42] and variational auto encoder (VAE) [43] to generate test inputs. Holistically speaking, a generative model is trained to map a seed dataset corpus to a continuous distribution, a.k.a., a unified latent space. Once trained, new inputs can be generated by sampling from the latent space. Since data are mapped to a continuous distribution, infinite samples can be generated as test inputs.

Note that these SOTA works are not effective in generating media inputs with high DIV and VAL. Kang et al. [14] focuses on generating images that “lie on the semantic *boundary* of labels.” They thus generate media data with obscurely defined labels (e.g., a fused digit of “4” and “9”), which is less useful for DNN testing when checking the prediction consistency. In Fig. 5(b), we present some examples generated by [14], whose key limitation is also pointed out by [15]. Instead, Dola et al. [15] samples media data “within distributions.” However, as will be proved in Sec. 4.2, these SOTA works are only applicable to toy datasets like MNIST, and VAL is deemed to be nullified when their methods are used for real-world images. We present examples in Fig. 5(b): when following their strategies to mutate images from ImageNet [44], only meaningless, broken images are generated. In contrast, DEEPWALK can generate meaningful and diverse images using ImageNet as the seed corpus, as shown in Fig. 5(c).

4 FORMAL ANALYSIS

In this section, we formally define VAL and DIV of a test suite based on manifold and show how they inextricably bound each other. We then demonstrate how to provably increase VAL and DIV.

4.1 DATAGEN: A Unified Formulation of Media Input Mutation/Generation Methods

We first formulate the input mutation (Sec. 3.1) and input generation (based on generative models; Sec. 3.3) meth-

ods of existing testing works as a unified data generation (DATAGEN) process.

Definition 1 (DATAGEN). *Given media data x , mutating x to \hat{x} , or generating \hat{x} from x , can be formulated as a unified data generation process $\hat{x} = G_{\theta_2}(E_{\theta_1}(x), h)$. E_{θ_1} is the encoder converting x into a (latent) representation. G_{θ_2} is the generator and $h \in H$ specifies how \hat{x} is different from x . $\theta_1, \theta_2 \in \emptyset \cup \Theta$ and Θ is the parameter space.*

θ_1 and θ_2 can be \emptyset , and therefore, most mutation-based DATAGEN introduced in Sec. 3.1 can be written as a non-parametric form $G(E(x), h)$, where $E(x) = x$, $h = [a, b]^T \in H$ and $G(E(x), h) = [x, 1] \times h = ax + b$. Concretely, for byte-level mutations, a and b are floating numbers. For example, to make a picture brighter, $a = 1.0$ and $b > 0$. For affine/convolutional transformations, a and b should be matrices/vectors, e.g., a is the rotation matrix and b is zero vector when rotating x . DATAGEN based on style transfer can be represented as $G_{\theta_2}(E(x), h)$, where $\theta_2 \in \Theta$ and $E(x) = x$. G_{θ_2} is the style translator, and $h \in H$ is the parameter that decides which and to what extent a style is transferred over x .

For SOTA generative model-based DATAGEN, $\forall x \in \mathbb{X}$, $E_{\theta_1}(x) \equiv \mathbb{Z}$, where \mathbb{X} is the pixel space and \mathbb{Z} is the low-dimensional representation of \mathbb{X} , e.g., the unified latent space of [14], or the ‘‘distribution’’ referred in [15]. Then, $G_{\theta_2}(\mathbb{Z}, h) = g_{\theta_2}(z \stackrel{h}{\sim} \mathbb{Z})$, where g_{θ_2} is the generator trained over images from different manifolds and $z \stackrel{h}{\sim} \mathbb{Z}$ denotes sampling z from \mathbb{Z} according to criterion h . Concretely, h in [14] aims to sample images ‘‘lying in distribution boundaries’’ whereas h in [15] samples ‘‘in-distribution’’ images.

In our work, DEEPWALK, $\hat{x} = G_{\theta_2}(E_{\theta_1}(x), h) = G_{\theta_2}(\mathcal{E}_{\theta_1}(x) \times h)$, where \mathcal{E}_{θ_1} is the encoder that converts x to its representation in the manifold and G_{θ_2} is the generator that maps from each manifold $\mathcal{M} \subset \mathbb{M}$ to its corresponding region in \mathbb{X} . Both \mathcal{E}_{θ_1} and G_{θ_2} consider the separation between manifolds. h is the perceptual transformation launched on each $\mathcal{M} \subset \mathbb{M}$ that mutates certain perceptions under feedback of some off-the-shelf DNN testing criteria. Based on Def. 1, we have the following two assumptions.

Assumption 1 (Gaussian Input). *The input of $G_{\theta \in \emptyset \cup \Theta}$ in DATAGEN (Def. 1) is sampled from a Gaussian distribution.*

Analysis of Assumption 1. Inputs of generative models, by design, are sampled from either uniform or normal distributions (i.e., a special case of Gaussian distribution). Because uniform distribution can be converted from Gaussian distribution [45], Theorem 1 holds for generative model-based DATAGEN.

For mutation-based DATAGEN, given an input x , all possible mutated images are $\hat{\mathbb{X}}_x \leftarrow [x, 1] \times H$.⁴ To our best knowledge, all prior works sample h based on either normal distribution or uniform distribution.⁵ For normal distribution, $h \sim \mathcal{N}(H_{\min} + \frac{H_{\Delta}}{2}, (I \cdot H_{\Delta})^2) = H_{\Delta} \cdot \mathcal{N}(H_{\min} + \frac{H_{\Delta}}{2}, I^2)$

4. $\hat{\mathbb{X}}_x \leftarrow G_{\theta_2}(x, H)$ for input mutation based on style transfer. In this section, we primarily discuss non-parametric input mutations whose conclusion can be directly extended to style transfer-based mutations.

5. In practice, the de facto image library, OpenCV [46], only provides sampling pseudo random numbers from normal or uniform distributions. OpenCV is extensively used by most, if not all, DNN testing research.

where $H_{\Delta} = H_{\max} - H_{\min}$ and I is the identity matrix. Therefore, $\hat{\mathbb{X}}_x \leftarrow [x, 1] \times zH_{\Delta}$ where $z \sim \mathcal{N}(H_{\min} + \frac{H_{\Delta}}{2}, I^2)$. The same applies if $h \sim H$ is based on uniform distribution. Therefore, for a given x and H , $\hat{\mathbb{X}}_x$ is generated by taking inputs z sampled from Gaussian distribution; Assumption 1 thus holds. In DEEPWALK, as will be shown in Sec. 5, since h is a covariance matrix and $\mathcal{E}_{\theta_1}(x)$ follows normal distribution, inputs to G_{θ_2} are accordingly samples from Gaussian distribution. \square

Assumption 2 (Lipschitz Constant). $\exists L > 0$, the Lipschitz constant of $G_{\theta \in \emptyset \cup \Theta}$ is no larger than L , i.e., $\forall (z_i, z_j)$ satisfy

$$\sup_{z_i \neq z_j} \frac{\|G_{\theta}(z_i) - G_{\theta}(z_j)\|}{\|z_i - z_j\|} \leq L$$

Analysis of Assumption 2. For non-parametric DATAGEN, as discussed in Analysis of Assumption 1, since $|G_{\theta}(z_i) - G_{\theta}(z_j)|/|z_i - z_j|$ is a constant, Assumption 2 is therefore always true.

For generative model-based DATAGEN, Assumption 2 should also hold since, conceptually, well-trained generative models are leveraged for DATAGEN, whose Lipschitz constants are bounded. Otherwise, $|G_{\theta}(z_i) - G_{\theta}(z_j)|/|z_i - z_j| \rightarrow \infty$, such that the generated images are corrupted — the generative models can hardly generate useful test inputs [47], [48]. On the other hand, in practice, various approaches for bounding the Lipschitz constant are adopted when training generative models, such as weight clipping, spectral normalization, etc [47], [48], [49], [50]. These approaches support Assumption 2 from a technical perspective. \square

4.2 Quantifying Perception VAL and DIV of Media Data Generated via DATAGEN

Def. 1 cohesively formulates existing media data mutation/-generation methods as DATAGEN. Inspired by the precision & recall criteria proposed by [51] for measuring generative models, we formulate VAL and DIV. Let the seed corpus be \mathcal{S} , which lie on a collection of manifolds $\mathcal{M} \subset \mathbb{M}$. Let the data generated (according to Def. 1) via G_{θ} from \mathcal{S} be $\hat{\mathcal{S}}_{\theta}$. Intuitively, VAL of $\hat{\mathcal{S}}_{\theta}$ can be quantified as the proportion of $\hat{\mathcal{S}}_{\theta}$ that lie in \mathbb{M} . Accordingly, DIV of $\hat{\mathcal{S}}_{\theta}$ can be quantified as the proportion of $\mathcal{M} \subset \mathbb{M}$ that is covered by $\hat{\mathcal{S}}_{\theta}$. Formally, we have the following definition.

Definition 2 (VAL and DIV). *Given corpus \mathcal{S} lying on manifolds \mathbb{M} with associated distribution \mathcal{P} (note that as introduced in Sec. 2.2, \mathcal{P} is discontinuous if multiple manifolds exist). Suppose test suite $\hat{\mathcal{S}}_{\theta}$ generated (see Def. 1) over \mathcal{S} has distribution \mathcal{Q} . Let $\Lambda = \text{supp}(\mathcal{P}) \cap \text{supp}(\mathcal{Q})$, where $\text{supp}(\mathcal{P})$ is the support of \mathcal{P} .⁶ Then, \mathcal{P} is the mixture of \mathcal{P}_{Λ} and $\mathcal{P}_{\bar{\Lambda}}$ which are distributions defined on Λ and the complement of Λ , respectively. Similarly, \mathcal{Q} can be defined over \mathcal{Q}_{Λ} and $\mathcal{Q}_{\bar{\Lambda}}$.*

Definition 2.1 (VAL α). $\hat{\mathcal{S}}_{\theta}$ has a validity score $\alpha \in [0, 1]$ such that $\mathcal{Q} = \alpha\mathcal{Q}_{\Lambda} + (1 - \alpha)\mathcal{Q}_{\bar{\Lambda}}$.

Definition 2.2 (DIV β). $\hat{\mathcal{S}}_{\theta}$ has a diversity score $\beta \in [0, 1]$ such that $\mathcal{P} = \beta\mathcal{P}_{\Lambda} + (1 - \beta)\mathcal{P}_{\bar{\Lambda}}$.

6. For the pixel space \mathbb{X} , $\text{supp}(\mathcal{P}) = \{x \in \mathbb{X} | \mathcal{P}(x) > 0\}$.

Validity vs. Diversity Based on theoretical results of [52], we have the following important Lemma.

Lemma 1 (The None Land). ⁷ For a generator G_θ that satisfies Assumption 1 and Assumption 2, suppose its generated test suite \hat{S}_θ captures \hat{K} manifolds, which are $\hat{\alpha}$ overlapped with the manifold collection \mathbb{M} . Let \mathbb{M} has total K disconnected manifolds, where $\hat{\beta}$ percentage is covered by \hat{S}_θ . Thus, $\hat{K} \geq K\hat{\beta}$ and

$$\begin{aligned}\hat{\alpha} &\leq \exp\left(\frac{1}{2}\left(\frac{D}{2L}\right)^2 + \frac{D}{2L}\sqrt{2\log\hat{K}}\right)^{-1} \\ &\leq \exp\left(\frac{D}{2L}\sqrt{2\log K\hat{\beta}}\right)^{-1}\end{aligned}$$

holds, where D is the minimal distance between any two manifolds and L is from Assumption 2. Importantly, when K is large (e.g., $K = 1,000$ for real-world media datasets like ImageNet), $\hat{\alpha}$ is negligible, with induced outputs provably falling into the “None” region (e.g., generated images are meaningless).

Interpretation. $\hat{\alpha}$ and $\hat{\beta}$ quantify perception VAL and perception DIV defined in Def. 2, respectively. It explains why SOTA methods can succeed on a toy dataset like MNIST by generating diverse images of convincing realism. MNIST has only 10 classes, corresponding to ten manifolds (i.e., $\hat{K} = 10$). Moreover, D , the minimal distance of two manifolds (e.g., manifolds for digits “4” and “9”), is small since every MNIST image comprises a white digit on a black background.

However, we point out that for real-world media datasets like ImageNet, D is often large. For example, what and how perceptions form a car are distinct with that of a dog. Also, with 1000 classes in ImageNet, \hat{K} is large (i.e., 1000) and α is suppressed to negligible, leading to “None” outputs. In sum, Lemma 1 illustrates a critical albeit overlooked limit of SOTA works:

The SOTA methods employ generative models for DATAGEN, which captures full manifolds of corpus \mathcal{S} in a unified distribution. However, when D and \hat{K} are large, VAL of generated data \hat{S}_θ is inevitably small, resulting in outputs falling into the “None” region. That is, when D and \hat{K} increase, samples generated by SOTA works would fall outside of \mathbb{M} and are meaningless.

Having that stated, previous non-parametric DATAGEN does not suffer from this problem since $\forall x \in \mathbb{X}, E(x) = x$; the transformed Gaussian inputs (see Def. 1) are separated by each input.

Viewing their pros and cons through the lens of manifold, our intuition is to explore the conceptual synergy of existing DATAGEN by *treating individual manifold separately*. This way, we limit K to a small value (K may be slightly over one since there may be estimation errors) and overcome the “The None Land” problem. Lemma 1 also shows that given D and K derived from the seed corpus \mathcal{S} , α and β inextricably bound each other, though the bound is *not* tight. For instance, when K is close to 1, the bound approximates

⁷ Lemma 1 is originally referred as “no GAN’s land” in [52]. Nevertheless, its theory is not limited to GAN (it only requires G satisfying Assumption 1 and Assumption 2) and we rename it as “the None Land” to better reflect our view.

1. This reveals opportunities to provably enhance DIV and VAL when generating media data, as will be discussed in Sec. 4.3.

4.3 Retaining VAL: A Mechanical Way

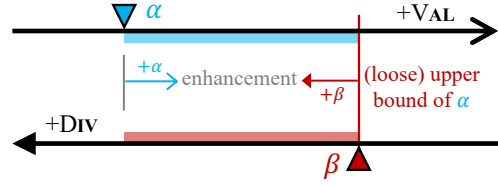


Fig. 6. Improving VAL and DIV due to the loose bound.

Lemma 1 shows α and β bound each other. Therefore, increasing DIV would reduce the upper bound of VAL, and vice versa. Nevertheless, we clarify that VAL can be retained to a reasonably high extent, if not improved, when increasing DIV. The reasons are two-fold. First, while β upper bounds α according to the “The None Land” theory, we find that the bound is loose in practice. For instance, when K is small (e.g., close to 1), the bound approximates 1, according to this theory. Thus, as seen in Fig. 6, α and β can be enhanced simultaneously. Second, since manifolds preserve the closeness among data points (see Sec. 2.2), the region in G_θ ’s input space where the closeness is likely violated is possibly out-of-manifold, denoting inputs breaching VAL and having no contribution to DIV. Therefore, we propose a mechanical way to retain high VAL, by identifying and pruning samples in \hat{S}_θ that have high local sensitivity. We first characterize the local sensitivity of a DATAGEN’s input.

Definition 3 (Sensitivity). For an arbitrary input z of G_θ , the Jacobian matrix J_{G_θ} of the generator G_θ with respect to z is defined as:

$$J_{G_\theta}(z)_{i,j} = \frac{\partial G_\theta(z)_i}{\partial z_j},$$

where $J_{G_\theta}(z)_{i,j}$ is the (i, j) -th entry of $J_{G_\theta}(z)$. Accordingly, the local sensitivity of z towards G_θ is characterized by the Jacobian Frobenius Norm (JFN):

$$\|J_{G_\theta}(z)\|_F^2 = \sum_i \sum_j (J_{G_\theta}(z)_{i,j})^2$$

The intuition is that, the local sensitivity around z can be characterized via its gradient [53], which describes how much the output changes w.r.t. input perturbations. Considering previous media data mutation methods, where each $x \in \mathbb{X}$ is formulated as $\tilde{x} \leftarrow [x, 1] \times zH_\Delta$ and z is regarded as the Gaussian input to G_θ , the local sensitivity of z , by following JFN, is thus only (positively) decided by $H_\Delta = H_{\max} - H_{\min}$. Furthermore, according to the theoretical and empirical results in [52], [50], we have the following lemma:

Lemma 2 (Out-of-Manifold). Let a collection of data \mathcal{S} generated by G_θ has the VAL score as α . Let $|\cdot|$ denote the size of a set. We select a subset S_1 with the highest sensitivity from \mathcal{S} , where $|S_1| = \tau|\mathcal{S}|$ and $\tau < 1 - \alpha$. Suppose the out-of-manifold data in S_1 forms a set $S_2 = \{x \mid x \in S_1, x \notin \mathbb{M}\}$, we have:

$$\tau(1 - \alpha) < \frac{|S_2|}{|\mathcal{S}|}$$

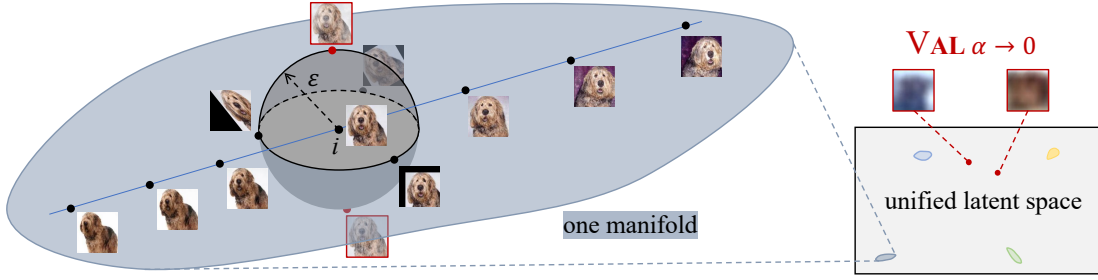


Fig. 7. Comparison between DEEPWALK and existing works by projecting their mutated images on manifold. Previous mutation approaches (left) can hardly mutate the perceptions. Similarly, existing input generation schemes (right), which do not consider the separation among manifolds, only generate meaningless inputs when applied on real datasets.

Lemma 2 demonstrates that when selecting data generated by DATAGEN with the highest sensitivity, the out-of-manifold data are more likely to be chosen. Therefore, by pruning these data, the VAL score α should be increased. Concretely, we present the following theorem:

Theorem 1 (Increasing VAL when Retaining DIV). *Given a collection of data samples S generated by G_θ whose VAL score is α and DIV score is β , we prune a proportion of τ samples, dubbed as S_1 , that have the highest sensitivity, where $\tau < 1 - \alpha$. Let $p|S|$ be the number of out-of-manifold samples in the pruned data (i.e., $|S_2|$ in Lemma 2), then we can compute the new VAL score α^\uparrow and DIV score β^\approx as follows:*

$$\alpha^\uparrow = \frac{\alpha - \tau + p}{1 - \tau}, \quad \beta^\approx = \frac{\alpha - \tau + p}{\alpha} \beta.$$

Lemma 2 trivially provides $p > \tau(1 - \alpha)$, and as a consequence, we have

$$\alpha^\uparrow > \alpha \quad \text{and} \quad \beta^\approx > (1 - \tau)\beta$$

According to Def. 3, the sensitivity of $G_{\theta \in \Theta}$ is measured by its JFN. Theorem 1 states that by pruning points having the highest sensitivity in manifolds, we can increase the VAL of data produced from DATAGEN. Moreover, this should not notably undermine DIV, given p , denoting percentage of out-of-manifold data, and τ , denoting percentage of samples with the highest sensitivity, are close. As a result, $\beta^\approx \approx \beta$. In particular, when α is high, τ becomes negligible (τ is less than 0.01 in our setup; see Sec. 6 and Sec. 7). This leads to a tight lower bound (close to β) for β^\approx . We present the full proof of Theorem 1 at the end of this section.

The Mechanical Procedure. As will be shown in Sec. 4.4, DIV can be largely increased by extensively exploring the manifold and performing DATAGEN. However, according to “The None Land” theory, the upper bound of the VAL score α is inevitably reduced (though not tight) when DIV increases. Therefore, to retain VAL, we prune a proportion of τ samples having the highest sensitivity from the outputs of DATAGEN following Theorem 1.

Reflection on Previous DATAGEN Setups. Key findings at this step can be used to rigorously explain previous DATAGEN setups. For instance, generative model-based DATAGEN would require to truncate the input space of the generator to improve the realism (VAL) of generated samples. For the non-parametric input mutation methods (i.e., G_θ), the sensitivity is only decided by $H_\Delta = H_{\max} - H_{\min}$.

Thus, to improve VAL, we can shrink the choices of h .⁸ Note that this is aligned with their current setups, e.g., limiting the number of the mutated pixels, as introduced in Sec. 3.2.

Proof of Theorem 1. For the data samples with the highest sensitivity $x \in S_1$, the proportion of out-of-manifold data is p , where $p = \frac{|S_2|}{|S|}$ and $\forall x \in S_2, x \in S_1$ and $x \notin \mathcal{M}$. The new VAL score α^\uparrow is calculated as below:

$$\begin{aligned} \alpha^\uparrow &= \frac{\alpha|S| - (|S_1| - |S_2|)}{|S| - |S_1|} = \frac{\alpha|S| - \tau|S| + p|S|}{|S| - \tau|S|} \\ &= \frac{\alpha - \tau + p}{1 - \tau} \end{aligned}$$

Similarly,

$$\begin{aligned} \beta^\approx &= \frac{\alpha|S| - (|S_1| - |S_2|)}{\alpha|S|/\beta} = \frac{\alpha|S| - \tau|S| + p|S|}{\alpha|S|} \beta \\ &= \frac{\alpha - \tau + p}{\alpha} \beta, \end{aligned}$$

according to Lemma 2, $p > \tau(1 - \alpha)$, we thus have

$$\alpha^\uparrow > \alpha, \quad \beta^\approx > (1 - \tau)\beta$$

□

4.4 Increasing Div: A Schematic Comparison

Our DATAGEN is implemented as a practical framework, namely DEEPWALK, whose full technical details are presented in Sec. 5. DEEPWALK mutates media data by walking on the corresponding manifold towards different directions and with varied step sizes. This enables diverse perceptual-level mutations and gradually increases DIV. Fig. 7 presents a schematic comparison of DEEPWALK and existing works. On a data manifold, a seed image i is mutated when DEEPWALK walks toward the bottom left and the top right. The footsteps of DEEPWALK, after being mapped back to the high-dimensional space, yield a succession of mutated images with perceptions changed.

Prior mutation-based works, as reviewed in Sec. 3.1, directly mutate media data. Their mutated images typically surround the seed i in an ε -radius sphere. Some mutated images breach the perceptual constraints (e.g., by adding too much random noise), thus residing outside the manifold (shown in red in Fig. 7; the red dot is on the sphere and above the manifold). Although these mutated images may trigger

⁸ Note that to enable diversified mutation patterns, H_{\min} is generally set to “ $-H_{\max}$ ” in their setting.

DNN mis-predictions, they typically stress only a limited range of behaviors of DNNs, given that perception changes are not comprehensively explored. Worse, we emphasize that the ε -radius must be *reasonably small*, as images may become unidentifiable, with disrupted senses, as ε rises. This conclusion can also be derived from Theorem 1. Sec. 3.2 described how existing methods retain “validity”; e.g., DeepHunter allows only one affine transformation per image. Thus, existing methods are confined within limited perceptions by design. Clearly, DEEPWALK can mimic existing mutations by limiting the step size as smaller than ε .

Fig. 7 also presents SOTA generative model-based methods, which map images belonging to different manifolds to a unified space. As illustrated in the “The None Land” theory, their methods are proved to only generate images of negligible VAL for real-world media data.

5 DESIGN OF DEEPWALK

Fig. 8 illustrates the high-level workflow of DEEPWALK, in terms of manifold construction (Fig. 8(a)) and feedback-driven testing (Fig. 8(b)). Sec. 5.2 and Sec. 5.3 will introduce these two phases respectively.

Application Scope and Position. DEEPWALK is designed as a DNN testing tool that mainly addresses issues in the input mutation/generation. More specifically, DEEPWALK seeks to improve the diversity of test inputs (which are achieved via perceptual-level mutations) given a limited number of seed inputs, thereby effectively and comprehensively studying DNN faults. Meanwhile, DEEPWALK also aims to retain the validity of test inputs when performing mutations, such that it discloses real DNN faults rather than those induced by invalid inputs (i.e., false positives).

Techniques in DEEPWALK are based on data manifold, which is approximated using generative models. Overall, DEEPWALK demonstrates the successful application of data manifold in DNN testing and does *not* focus on proposing new methods for forming manifold. DEEPWALK provides an out-of-box solution to leveraging generative models to get (disconnected) manifolds for real-world media data with different formats, in a unified way. The core techniques of DEEPWALK are agnostic to the implementation of generative models or the format of media data.

We leverage GANs [42] in the current implementation of DEEPWALK and discuss the design consideration in Sec. 5.1 (see **Generative Models**). Given that said, we clarify that DEEPWALK is not specifically designed for GANs. Users may replace our employed GAN with more advanced generative models, if needed. This should be technically feasible: users only need to replace the mapping function between media data and manifolds with that in the new generative models.

5.1 Manifold in DNN Testing

A manifold can be constructed by finding a projection $f_\theta : \mathcal{R}^9 \rightarrow \mathcal{M}$ that converts media data $x \in \mathcal{R}$ into $z = f_\theta(x)$ on \mathcal{M} . That said, mapping $f_\theta(x) \in \mathcal{M}$ back to $x \in \mathcal{R}$ requires the reconstructed data to be realistic. Also, $f_\theta : \mathcal{R} \rightarrow \mathcal{M}$ is often approximated on a limited number of data. This raises practical challenges to construct an

expressive manifold that can facilitate synthesizing diverse $x \in \mathcal{R}$. It is shown that employing generative models can construct manifolds [18], [54], [55]. In general, these generative models are parameterized and enable “learning” data manifold from usually limited data samples. This makes generative models a desirable choice for DNN testing where the seed inputs are typically limited.

Generative Models. Various paradigms of generative models are proposed in past few years. For examples, variational auto-encoder (VAE) [43] jointly trains an encoder and a decoder to form a bidirectional mapping between media data and manifold. Nevertheless, outputs of VAE suffer from the over-smooth issue [56]. Image details such as edges and textures typically vanish during the generation procedure, which will harm the effectiveness of DNN testing. Flow-based [57] and Diffusion [58] models adopt (mathematically) invertible modules to build the generative model. For flow-based models, image quality remains a major concern, and they do not have a low-dimensional latent space (the dimensions of latent space equal the image size, i.e., $\#channels \times width \times height$). Also, despite diffusion models can generate vivid and realistic images, their training requires billions of training data. For instance, Stable Diffusion [59] is trained on 5 billion images. We note that prior testing tools in this field and DEEPWALK share a common design focus to effectively use (usually limited) available seed inputs. Thus, employing Diffusion model indeed introduces a dilemma for this setting: once developers have enough training data (i.e., the seed inputs), they may no longer need to train the Diffusion model, as they can directly use these billions of data (which are more than sufficient) to test the target DNN. Moreover, collecting such a huge number of training data may be likely infeasible for testing DNNs in various real-world, specialized domains, e.g., medical image diagnosis or autonomous driving.

Therefore, DEEPWALK chooses generative adversarial nets (GANs) [42] to form data manifold. Compared with VAE, GANs can generate images of higher quality. It also requires much less training data than Diffusion models. A potential limitation is that a GAN only contains one generator (decoder) that has maps $\mathcal{M} \rightarrow \mathcal{R}$; it does not provide an encoder for $\mathcal{R} \rightarrow \mathcal{M}$. In Sec. 5.2, we introduce how we build encoders for GANs.

Requirement for Dataset. Fig. 8(a) shows the offline phase of DEEPWALK which prepares a manifold over dataset \mathcal{S} . DEEPWALK mutates media data of different types. We use a GAN to create a specific manifold over \mathcal{S} , which can be images, audio, or text. We assume that \mathcal{S} represents all accessible data for DNNs testing. In our evaluations (see Sec. 7), we use training data of the tested DNN as \mathcal{S} to simulate testing conducted by the DNN developer. For general real-world users of DEEPWALK, they may use any public/private dataset they have as \mathcal{S} .

Data Representation. Media data can be categorized into two types: continuous and discrete. Image and audio data are continuous since they are composed of floating numbers. Images are formed as $\#channels \times width \times height$ matrices and their manifolds can be constructed directly on this representation (see below). It is, however, challenging to capture perceptual constraints of audio in the raw format (e.g., .wav). Generally, audio can be converted into 2D

9. Here we use \mathcal{R} to for media data of different formats, including image, text, and audio.

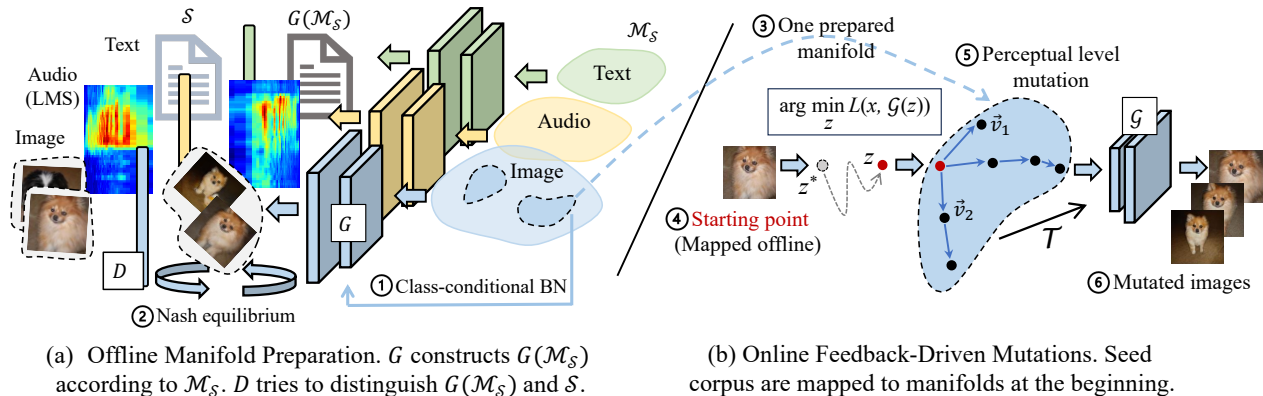


Fig. 8. Workflow of DEEPWALK, which is unified for image, audio, and text. In the offline phase, DEEPWALK first constructs manifolds using GAN. It leverages class-conditional batch normalization to handle the separation among different manifolds. This process is finished when the generator G and discriminator D establish a Nash equilibrium. In the online phase, DEEPWALK performs perceptual mutation in each manifold with a footprint-aware manner. Guided by the testing objectives, DEEPWALK mutates certain perceptions that likely trigger DNN faults.

forms, representing the acoustic information as frequency series along the time and further transformed back to the original ones losslessly. That is, an audio can be represented as an “image” of size $1 \times frequency \times time$. Our evaluation shows that the *image-style* representation is expressive, given that audio contents and intonations can be characterized via frequencies, whose changes alter the formed images in a constrained way. Thus, we convert audio into the log-amplitude of Mel spectrum (LMS; see Fig. 8(a)) and construct their manifolds as for images. Textual data comprise a sequence of words. They are discrete because there is no “intermediate word.” As noted in Sec. 2.2, the word dependencies encode the semantics and grammatical coherence of a sentence, which are the primary focuses of their derived manifolds. Nevertheless, it is infeasible to directly compute the manifold of text using GAN. We use ARAE [60], a prominent approach that uses adversarial regularization, to convert discrete text into a continuous representation, enabling to process text data with a GAN.

5.2 Offline Manifold Preparation

Preparing Manifolds via GANs. GAN employs generator network G and discriminator network D , with the objective to make data approximated by G indistinguishable under the view of D . GAN minimizes the “distance” between real and synthesized data distributions. It seeks a Nash equilibrium in a two-player zero-sum game:

$$\min_G \max_D \mathbb{E}_{x \sim \mathcal{R}} [\log D(x)] + \mathbb{E}_{z \sim p(z)} [\log(1 - D(G(z)))]$$

where z is a vector of much lower dimensions and is sampled from a continuous distribution $p(z)$, which is typically set as $\mathcal{N}(0, I)$. G implicitly encodes constraints formed by real data. DEEPWALK first launches an offline phase to train GAN, including generator network G and discriminator network D , over a set of media data. Only G is used in the follow-up online testing. The training is finished until G can constantly generate diverse and valid media data instances. **Handling Distinct Manifolds.** Both G and D are composed of stacked blocks [61]. Each block has a convolutional layer, a batch normalization (BN) layer [62] and a non-linear

function. The BN layer acts as a regularizer by normalizing a batch of input for subsequent layers as

$$x = \frac{x - Mean}{\sqrt{Var}} \gamma + \mu$$

with learned gain γ and bias μ , where $Mean$ and Var are the mean and variance of all $x \in \mathcal{R}$, respectively. It alleviates the problem of *internal covariate shift*, which refers to the varied distribution of input for each layer during training, thus guaranteeing G and D to be of saturating nonlinearity [62].

Data of different classes lie in distinct manifolds (e.g., dog vs. vehicle images); therefore, it is generally infeasible to design a universal model to construct distinct manifolds, as proved in Lemma 1. Without training a separate model for each manifold (which is computation-intensive), we use class-conditional BN to alleviate this hurdle [63], [50]. The gain and bias in each BN layer depend on the manifold to be constructed. And accordingly, the input to G is the concatenation of a latent vector z and a class label¹⁰ of the target manifold. As illustrated in Fig. 8(a), we only need to switch between BN layers to transit across distinct manifolds. Aligned with Sec. 4, we denote the G , which considers the separation among manifolds via class-conditional BN, as \mathcal{G} in the rest of this paper. Accordingly, the corresponding encoder is dubbed as $\mathcal{E} = \mathcal{G}^{-1}$.

Per-Input GAN Inversion for $\mathcal{R} \rightarrow \mathcal{M}$. A potential solution to getting $\mathcal{E} = \mathcal{G}^{-1}$ in GANs is building a universal encoder (which can map all data to the manifold) for a GAN’s generator. Nevertheless, this strategy is costly (since it almost doubles the original training cost) and also unnecessary. Intuitively, before online testing, we only need to map the seed inputs onto their coordinates in the manifold. Thus, to reduce the cost, we propose to implement GAN inversion in a per-input granularity. Instead of building an encoder (as in VAE), we re-form the inversion for an input (or a batch of inputs) as an optimization task which can be solved using DNN training optimizers such as SGD [64] or Adam [65].

10. To ease reading, we omit the class label when presenting the generator’s input in the rest of this paper.

For a seed input x , GAN inversion aims to find its coordinate $z \sim p(z)$ in the manifold such that $L(x, \mathcal{G}(z)) < \epsilon$, where L is the distance metric. This procedure can be formulated as the following:

$$\mathcal{E} : \mathcal{G}^{-1}(x) = \arg \min_z L(x, \mathcal{G}(z))$$

To implement this, we start with a randomly selected z^* . The optimizer then updates z^* to z to minimize $L(x, \mathcal{G}(z))$. The overall procedure is similar to DNN training, but the optimizer is applied on z (not DNN parameters). Since the latent space is much smaller than the parameter space of a DNN, inverting GAN in a per-input granularity yields significantly less cost than training an encoder.

Once $z = \mathcal{G}^{-1}(x)$ is obtained, by assigning a walking direction and a step size, DEEPWALK walks from z to z' . z' will be fed to \mathcal{G} , a decoder $f_\theta^{-1} : \mathcal{M} \rightarrow \mathcal{R}$, that maps z' back to realistic and valid high-dimensional media data $\mathcal{G}(z')$. Different walking directions will lead to different perception changes and the step size decides the changing extent. Since $p(z)$ is continuous, DEEPWALK can walk with an infinitely small step size.

5.3 Online Feedback-Driven Mutation

Fig. 8(b) illustrates the online phase of DEEPWALK, with the key algorithm in Alg. 1. The offline phase has mapped a seed corpus \mathcal{S} to coordinates \mathcal{C} (using \mathcal{E} which considers the separation among different manifolds) on manifold. A priority queue \mathcal{Q} is initialized using all elements with equal priority in \mathcal{C} ; each seed c in \mathcal{Q} may be used as the starting point for several walking iterations, unless its priority is lower than a threshold. The reason for keeping each seed coordinate c for multiple iterations is that mutating different perceptions on the same data (e.g., images) is likely to trigger different DNN behaviors.

Also, not all mutations can trigger new DNN behaviors — mutating c many times is unlikely to reveal new faults. Therefore, we lower the priority of c progressively (line 12) and spend more efforts on other seeds in \mathcal{Q} .

Retaining VAL. Before explaining the online phase presented in Fig. 8(b), we first discuss how to retain VAL in online testing. As clarified in Sec. 4.3, extensive mutations, though increasing DIV, can undermine VAL of produced samples. Accordingly, Sec. 4.3 presents a mechanical approach to retaining VAL by discarding samples with high local sensitivity on manifolds. To do so, once samples in the seed corpus are mapped to their manifolds, we record the maximal JFN, dubbed η_m , of all seeds (line 7 in Alg. 1; recall that JFN characterizes the local sensitivity of seeds). Then, during mutations, a mutated seed (or a randomly sampled coordinate; see line 14) will be kept for further mutation only if its JFN is no larger than η_m (line 16).

Exploitation vs. Exploration. Our mutation is inspired by “exploitation vs. exploration” [66], a popular paradigm that enables random exploration (to uncover new knowledge) and exploits knowledge learned from previous footprints. At time step t , we may (with probability λ) mutate a seed c with the highest priority in \mathcal{Q} (lines 9–12). This way, DEEPWALK walks from c to c_t as $c_t = c\mathcal{T}$ where \mathcal{T} denotes the *direction*, and its cardinality is the *step size*. \mathcal{T} is a covariance matrix calculated over previous footprints taken

Algorithm 1: Footprint-Aware Mutation.

```

1 Fuzzing Seed:  $\mathcal{C}$ ; // coordinates on  $\mathcal{M}$ ; mapped via  $\mathcal{E}$ 
2 Priority Queue:  $\mathcal{Q}$ ;
3 Generative Model:  $\mathcal{G}$ ;
4  $\mathcal{Q} \leftarrow \mathcal{C}$ ;
5  $\lambda \leftarrow 0, t \leftarrow 1$ ;
6  $\mu_0 \leftarrow 0, \mathcal{T}_0 \leftarrow 0$ ;
7  $\eta_m \leftarrow \max_{c \in \mathcal{C}} J(c)$ ; // record maximal JFN
8 while not can_terminate() do
9   if uniform(0, 1)  $\leq \lambda$  then
10      $c \leftarrow \mathcal{Q}.select()$ ;
11      $c_t \leftarrow c\mathcal{T}_{t-1}$ ; // footprint-aware mutation
12      $\mathcal{Q}.decrease\_priority(c)$ ;
13   else
14      $c_t \leftarrow sample\_from\_manifold()$ 
15   end
16   if  $J(c_t) < \eta_m$  and objective( $\mathcal{G}(c_t)$ ) then
17      $\mu_t \leftarrow \frac{t-1}{t}\mu_{t-1} + \frac{c_t}{t}$ ;
18      $\mathcal{T}_t \leftarrow \frac{(t-1)\mathcal{T}_{t-1}}{t} + \frac{(t-1)(\mu_{t-1}-c_t)(\mu_{t-1}-c_t)^T}{t^2}$ ;
19      $t \leftarrow t + 1$ ;
20      $\mathcal{Q}.add(c_t)$ ;
21      $\lambda \leftarrow \min(\lambda + \delta, \Lambda)$ ; // exploit vs. explore
22   end
23 end

```

on a manifold during the current online phase, representing the learned knowledge. DEEPWALK may also perform random exploration by randomly walk to c_t sampled on the manifold with a probability $1 - \lambda$ (line 14).

Random exploration may trigger new findings that challenge DNN predictions. Then, through repetitive explorations, \mathcal{T} gradually converges to directions that reflect effective perception changes (revealing new DNN behaviors). Thus, we expect that mutations according to \mathcal{T} may induce more oriented explorations of perception changes on the manifold and trigger more DNN behaviors (thus more likely to reveal DNN faults) in a given time budget. Consider the manifold in Fig. 8(b). If the testing objective (line 16) is neuron coverage, suppose that c has been mutated twice using \vec{v}_1 and \vec{v}_2 , which induces the activation of distinct groups of neurons in the target DNN, namely g_1 and g_2 . As DEEPWALK maintains \mathcal{T} , subsequent mutations over c will use $\vec{v}_1 + \vec{v}_2$, and therefore, mutations directing to $\vec{v}_1 + \vec{v}_2$ probably stress neurons interleaving with g_1 and g_2 .

Controlling the Trade-off. The trade-off between exploitation vs. exploration is controlled using δ and Λ (line 21). Starting from 0, λ is increased by δ each step if the testing objective is satisfied (line 16), e.g., coverage increase, until it reaches the predefined threshold Λ . This will gradually reduce the effect of randomness in determining walking directions and step sizes. With a large δ , the online mutation will quickly converge to exploitation but may not learn useful knowledge from a few explorations. However, if δ is too small, the online phase will be dominated by random explorations. Although it may comprehensively explore DNN behaviors, such knowledge cannot be timely exploited for oriented mutations. In addition, λ is not allowed to exceed Λ ($\Lambda < 1$) to retain chances of finding new useful

directions and step sizes on the manifold. $1 - \Lambda$ decides the minimal ratios of random exploration in the online phase; Λ should be set as a relative high value to avoid harming the exploitation. Meanwhile, we do not expect a too large Λ as it will eliminate exploring new DNN behaviors. See Sec. 6 for value suggestions of our employed hyperparameters.

Footprint-Aware Mutation. Given each coordinate c_i on the manifold as a vector, we keep track of all covered footsteps by using a *covariance matrix* \mathcal{T} . In lines 9–12, DEEPWALK mutates c using \mathcal{T}_{t-1} , which records the footsteps taken on this manifold until time $t - 1$. \mathcal{T} , as a matrix, is initialized to 0. If the media data $\mathcal{G}(c_t)$ derived from step c_t increases the DNN testing objective, DEEPWALK adds c_t to \mathcal{Q} and updates \mathcal{T} as follows:

$$\mathcal{T}_t = \frac{(t-1)\mathcal{T}_{t-1}}{t} + \frac{(t-1)(\mu_{t-1} - c_t)(\mu_{t-1} - c_t)^\top}{t^2}$$

where $\mu_{t-1} = \frac{1}{t-1} \sum_{i=1}^{t-1} c_i$ and will be updated as $\mu_t = \frac{t-1}{t} \mu_{t-1} + \frac{c_t}{t}$. The implementation of \mathcal{T} is an incrementally updated (using each c_i) covariance matrix. From a holistic view, \mathcal{T} encodes the direction and the corresponding step size on the manifold that are prone to satisfy DNN testing objective, according to experience collected until time t .

\mathcal{T} is initialized for each online phase. Effective walking directions and step sizes (i.e., better enhancing DNN testing criteria) require a \mathcal{T} that is specific for a manifold and the target DNN. For instance, to test an image classifier m_1 that relies on the ear shape to classify dogs, it would be beneficial to mutate perceptions related to the ear within manifold \mathcal{M}_{dog} over dog images. In contrast, to test an object detector m_2 , mutating perceptions related to motions (e.g., standing vs. lying) within \mathcal{M}_{dog} may better stress m_2 . Furthermore, Sec. 2.1 has introduced the *translation invariance* property of a CNN. Thus, \mathcal{T} helps to *adaptively* recognize certain perceptions that are prone to enhance DNN testing objective and reveal new behaviors, and it saves efforts mutating certain perceptions that have been shown as less effective based on current online phase experience.

6 IMPLEMENTATION & EVALUATION SETUP

DEEPWALK has about 2,100 LOC (counted by cloc [67]). DEEPWALK is written in PyTorch 1.9.0. Both online and offline phases of DEEPWALK are launched on one Intel Xeon CPU E5-2683 with 256GB RAM and one Nvidia GeForce RTX 2080 GPU.

Configurations. For the current implementation of DEEPWALK, we set δ and Λ as 0.0005 and 0.8, as two parameters in our exploitation (see Alg. 1), respectively. As explained in Sec. 5.3, these two parameters decide the trade-off between exploitation vs. exploration; we recommend users setting δ to a small value (e.g., around 0.001) and Λ to a relatively large value (e.g., within [0.75, 0.95]). Also, as mentioned in Sec. 5.2, media data of different sizes are mapped to manifold of different dimensions; we introduce the details in each corresponding section in Sec. 7. For inverting \mathcal{G} as in Sec. 5.2, we use Adam optimizer with a learning rate 0.002.

Pruning via Sensitivity. As in Alg. 1, we prune a mutated input if its JFN (see Def. 3) is higher than the maximal JFN among seed corpus. In our experiments, we find that less than 1% mutated inputs are pruned, i.e., $\tau < 0.01$

in Theorem 1. We interpret the findings as encouraging; according to the discussion associated with Theorem 1, DIV is preserved, and our mutations have high VAL.

6.1 Baselines

The target DNNs and the involved datasets are introduced in each experiment in Sec. 7. DEEPWALK is compared with representative tools reviewed in Sec. 3. To generate diverse and valid images at their best effort, all of these tools are configured with some key hyper-parameters. We list their setups as follows:

Generative Model-Based: [14] and [15] convert all images into a unified latent space and do *not* consider the separation of real manifolds. As proved in Sec. 4.2, they have negligible VAL for real images. We configure and test them using two popular real-world image datasets, ImageNet and CIFAR10. We report that they only generate images of meaningless color blocks (see some examples in Fig. 5(b)). As clarified previously, no universal perceptual constraints apply to all images [23], [17], e.g., what and how perceptions constitute a car does not apply to portraits. We thus skip comparing with them in the following experiments.

DeepHunter [13] requires that #mutated pixels is less than $a \times \text{\#total pixels}$, or the maximal value of changed pixels is less than $b \times 255$. We follow its default setting where $a = 0.02$ and $b = 0.2$.

TensorFuzz [5] truncates the accumulated noise within L_∞ . We use its shipped configuration which sets L_∞ to 0.4.

DeepSmart [20] mutates one small region of an image each time. We follow its default setting where #regions is nine. Since it does not explicitly preserve validity of mutated images, we use the image validation scheme of DeepHunter. **DeepTest** [3] rules out likely-broken mutated images based on the mean squared error (MSE). Given an image i and the mutated output i' , we only keep i' satisfying $MSE(i, i') < 1000$. Setting MSE as 1000 denotes a large and tolerable configuration with pixel values in [0, 255].

DeepRoad [4]/**TACTIC** [34] is specifically designed for testing autonomous driving. We reuse its released model to mutate driving scenes.

6.2 Testing Objectives

We benchmark DEEPWALK and the previous testing tools using different testing objectives, as introduced below.

Structural Coverage: Discrete states over neuron outputs are defined in structural neuron coverage. When being used as testing objectives, they guide the testing to maximize the covered states (i.e., neuron coverage). Compared with other testing objectives, structural neuron coverage can *reflect the testing comprehensiveness* as it offers interpretable values within [0, 100%], which quantify the explored DNN behaviors. We consider the following representative structural coverage due to their high computational efficiency¹¹. **Neuron Coverage (NC)** [2] rescales neuron outputs from the same layer to [0, 1]: a neuron is activated if its scaled output is greater than a threshold T . Same with [13], [20], we set T as 0.75.

K-Multisection Neuron Coverage (KMNC) [69] decides the normal output range of each neuron using all training data.

11. Their speed can be boosted via matrix computation; we use the optimized implementations provided by [68].

TABLE 1
Tested DNN models used in Sec. 7.

Model	#Neuron	#Layer	Remark
ResNet50 [70]	26570/27560*	54	Non-sequential topology
VGG16 [38]	12426/13416*	16	Sequential topology
MobileNet-V2 [71]	17066/18056*	53	Mobile devices
Inception-V3 [72]	10250/11240*	121	Feature extraction
DenseNet121 [73]	17018/18216*	95	Extremely deep model
Dave _{orig} [2]	1561	10	Autonomous driving
Dave _{norm} [2]	1561	10	Autonomous driving
Dave _{dropout} [2]	733	7	Autonomous driving
Transformer _{E2G} [74]	168386	328	Machine translation
Transformer _{G2E} [74]	168386	328	Machine translation
Audio CNN [75]	1610	7	Audio classification
QMobileNet _{Conv} **	18056	53	Quantized Conv layer
QMobileNet _{FC} **	18056	53	Quantized Conv layer
QMobileNet _{Conv+FC} **	18056	53	Quantized Conv&FC layer

*ImageNet version; each of the first five DNNs has two variants trained on ImageNet and CIFAR10.

** Three QMobileNet are black-box.

It then divides output range of each individual neuron into K -sections. The coverage is computed as how many (ratio) neuron outputs lie in the total $\#neuron \times K$ sections. Following DeepHunter, we set K as 1000.

Neuron Boundary Coverage (NBC) [69] calculates coverage by counting $\#neuron$ whose output lies outside the range decided in KMNC.

Strong Neuron Activation Coverage (SNAC) [69] deems a neuron as activated if its output is greater than the upper bound of the output range decide in KMNC.

Top- K Neuron Coverage (TKNC) [69] measures ratio of neurons in a layer appearing in the top- K outputs. We set K to 10.

Cluster-Based Coverage. The TensorFuzz paper also proposes a cluster-based coverage metric for DNN testing, which is often dubbed as TensorFuzz Coverage (TFC) [5]. Different from structural coverage that focus on neurons and their states, TFC treats all neuron outputs in a DNN as one high-dimensional vector v . During testing, a new cluster is formed if the distances between a new v and the center of its nearest cluster is greater than T ; the coverage is counted as the number of clusters formed by a test suite. Unlike structural coverage that set 100% as the maximal coverage value, TFC does not have a maximal coverage ($\#clusters$). In Sec. 7, we set $T = 5$ and $T = 500$ for DNNs trained on CIFAR10 and ImageNet, respectively.

Distribution-Aware Coverage. Neural coverage (NLC) [19] defines the coverage over distribution formed by layer outputs of a DNN. Similar to TFC, NLC also does not set a maximal coverage; it guides the testing to maximize the coverage value. Despite being less interpretable than structural coverage, NLC manifests better capability to reflect the diversity of test inputs and is more effective to guide generating error-triggering inputs (see our results in Sec. 7). NLC does not have hyperparameter.

Black-box Entropy. The above objectives are only available for white-/gray-box testing. Thus, we also consider a black-box testing objective to perform evaluation under a black-box setting, where only DNN outputs can be observed during testing. This objective measures the entropy between DNN outputs w.r.t. the original input and the mutated inputs. It guides the testing to maximize the entropy. The black-box entropy is also hyperparameter-free.

TABLE 2
Datasets used in Sec. 7.

Dataset	Format	#Class	#Sample	Size (Per-input)
CIFAR10 [76]	Image	10	50,000	$3 \times 32 \times 32$ pixels
ImageNet* [77]	Image	100	100,000	$3 \times 128 \times 128$ pixels
CityScape [78]	Image	N/A	2,759	$3 \times 256 \times 128$ pixels
SNLI [79]	Text	N/A	570,000	10–20 words
SC09 [80]	Audio	10	18,620	~1000 ms

*We randomly select 100 classes and rescale the size to 128×128 for speedup.

6.3 DNNs and Datasets

Table 1 lists the 19 DNNs tested in our evaluation.

General DNNs. The first ten DNNs (i.e., ResNet–DenseNet with each of them trained on two datasets) perform general image classification. They are representative in terms of the structure and topology (e.g., depth, sequential vs. non-sequential), featured platform (e.g., MobileNet is specifically designed for mobile devices), and the common utility (e.g., Inception’s outputs are commonly employed to construct similarity metrics for images).

Specialized DNNs. The next six DNNs are widely adopted in more specialized tasks for different formats of media datasets. The three variants of Dave models predict steering angles for driving scenes (i.e., a regression task). Transformer (which is the building block of recent large language models) takes natural language sentences as inputs and performs machine translation (e.g., translates English/German to German/English). Audio CNN is provided by [75] and recognizes the contents of audios of human voices.

Black-Box DNNs. The last three DNNs are different variants of quantized MobileNet. They are deployed in mobile devices and deemed as black-box because only DNN outputs (i.e., the predicted probability of all classes) are accessible. Testing these DNNs can demonstrate the generalizability of DEEPWALK in black-box scenarios.

Datasets. Table 2 lists the 5 datasets considered in the evaluation. The first three are image datasets. In particular, CIFAR10 and ImageNet are large-scale real-world datasets for general image understanding. CityScape contains 2,759 images taken from the driver’s view. SC09 features 18,620 sound clips of human voices saying numbers from 0 to 9. Each clip has a duration of about 1K ms and one number is said. The Stanford Natural Language Inference (SNLI) dataset contains 570,000 human-written English sentences. SNLI is commonly used for natural language inference and is grammatically coherent.

7 EVALUATION

We evaluate DEEPWALK by investigating the following research questions (RQs): **RQ1 (Effectiveness):** Is DEEPWALK more effective than previous tools? **RQ2 (Quality):** Can DEEPWALK generate test inputs of higher quality? **RQ3 (Generalizability):** Can DEEPWALK be generalized to different media data, tasks, and working scenarios? These three RQs are studied in Sec. 7.1–Sec. 7.3, respectively.

7.1 RQ1: Effectiveness

To answer **RQ1**, we evaluate the effectiveness of input mutation and validation in DEEPWALK and previous tools. For different input mutation strategies, we study if their generated inputs can comprehensively trigger DNN be-

TABLE 3
Ratios of invalid images without explicitly format restrictions.

	DEEPWALK	DeepHunter	TensorFuzz	DeepSmart	DeepTest
Invalid	0	76.96%	54.37%	77.23%	41.17%

TABLE 4
Testing comprehensiveness (%) before \rightarrow after excluding format-invalid images for ResNet trained on CIFAR10.

Init.	NC	KMNC	SNAC	NBC	TKNC
	55.39	1.43	0	0	23.21
DEEPWALK	64.37 \rightarrow 64.37	2.98 \rightarrow 2.98	3.27 \rightarrow 3.27	5.99 \rightarrow 5.99	26.24 \rightarrow 26.24
DeepHunter	61.85 \rightarrow 60.62	7.29 \rightarrow 3.99	3.15 \rightarrow 0	3.15 \rightarrow 0	25.38 \rightarrow 24.43
TensorFuzz	56.55 \rightarrow 56.21	2.94 \rightarrow 1.52	3.23 \rightarrow 0	3.23 \rightarrow 0	23.51 \rightarrow 23.38
DeepSmart	60.85 \rightarrow 58.94	6.85 \rightarrow 2.74	3.07 \rightarrow 0	3.07 \rightarrow 0	24.92 \rightarrow 23.86
DeepTest	57.18 \rightarrow 56.89	2.98 \rightarrow 2.98	1.54 \rightarrow 0	1.54 \rightarrow 0	23.68 \rightarrow 23.55

* "Init." denotes coverage achieved by seeds. Results are averaged over 5 runs with maximum standard deviation $< 10^{-3}$ (i.e., 0.0x%).

haviors and disclose more DNN faults. For input validation schemes, we evaluate whether they can faithfully rule out invalid inputs. We also benchmark the effectiveness of DEEPWALK’s design considerations (i.e., the footprint-aware mutation) via ablation studies.

Settings. Following previous works [13], [20], [5], we focus on image classification. We use CIFAR10 and ImageNet in this section. The dimensionality of each manifold is 120. At this step, training GAN takes one day for ImageNet (due to large volume of data) and 2 hours for CIFAR10. We release our trained models in [1]. All tested DNNs of CIFAR10 reach competitive test accuracy over 93%. ImageNet-trained DNNs are shipped by PyTorch. We use all training data of CIFAR10/ImageNet as the seed corpus for mutation or manifold construction. That is, all prior tools and DEEPWALK have the same data source and DEEPWALK is *not* empowered by more data. Overall, prior tools and DEEPWALK are compared to see which one enables more effective mutations by utilizing the same seeds. We let all tools run T hours and T is set to 6 and 4 for DNNs trained on ImageNet and CIFAR10, respectively. We set all tools to perform at most 50 mutations on an image in one iteration.

Objectives & Criteria. When being used as the testing objective, the five structural coverage metrics (see Sec. 6.2) are mainly adopted for reflecting the testing comprehensiveness because they provide interpretable numbers for the covered states of neurons. To study the disclosed DNN faults, we use NC (as one representative structural coverage¹²), TFC, and NLC as the testing objectives.

7.1.1 Input Validation

As introduced in Sec. 3.2, existing tools use heuristics to ensure the realism of mutated images. Nevertheless, we find that their heuristics may overlook images violating legit formats of RGB images (i.e., pixels values must lie in $[0, 255]$), let alone perception VAL.

Format-Invalid Inputs. For each testing tool, we count how many format-invalid images are overlooked by merely using its input validation scheme (without explicit considering

12. Other structural coverage metrics, such as SNAC and NBC, can hardly guide generating error-triggering inputs (prior tools have zero coverage increase under these metrics; see Table 6). This issue was also pointed out in one recent work [19].

TABLE 5
Disclosed DNN faults (#) before \rightarrow after excluding format-invalid images for ResNet trained on CIFAR10.

	NC	NLC	TFC
DEEPWALK	4073 \rightarrow 4073	21675 \rightarrow 21675	1309 \rightarrow 1309
DeepHunter	3219 \rightarrow 2011	18371 \rightarrow 7446	947 \rightarrow 740
TensorFuzz	95 \rightarrow 40	2726 \rightarrow 1879	40 \rightarrow 24
DeepSmart	511 \rightarrow 283	19196 \rightarrow 10196	256 \rightarrow 120
DeepTest	1020 \rightarrow 697	2172 \rightarrow 1007	1.54 \rightarrow 411

the format restrictions). Table 3 presents the ratios of format-invalid images generated by prior tools when mutating images from ImageNet. The percentages are high for all existing tools, indicating the ineffectiveness of their validation schemes and their mutations that directly operate on image pixel bytes. DEEPWALK, in contrast, mutates perceptions of media data, which by design would not break the format.

Misleading Testing. These neglected format-invalid images can be misleading as they can falsely manifest a high testing comprehensiveness and also report some false DNN faults. To unveil this issue¹³, we study how the testing comprehensiveness and #faults change after filtering out format-invalid images. Results are given in Table 4 and Table 5, respectively. As noted, the testing comprehensiveness and #faults is reduced considerably in previous tools. While this issue can be easily fixed by truncating the pixel values within $[0, 255]$ for RGB images, it is far more challenging for media data of complex formats (e.g., audios) where domain expertises are required. These observations highlight the superiority of perceptual-level mutations implemented in DEEPWALK, given that it is unified and agnostic to certain format restrictions. We further evaluate the perception validity VAL in Sec. 7.2.

7.1.2 Input Mutation Strategies

Testing Comprehensiveness. Table 6 reports the increased (structural) coverage of different tools, which can reflect the testing comprehensiveness achieved by different input mutation strategies. As just noted in Sec. 7.1.1, prior tools can yield format-invalid images but pass their validation. DNNs do not feature “format checking.” These format-invalid images, when being fed to DNNs, can falsely increase coverage value. To clarify, we exclude coverage due to invalid images and report the recalculated values in Table 6.

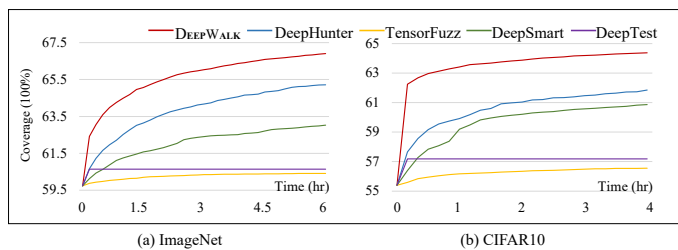


Fig. 9. Coverage (NC) increase of different tools on ResNet-50.

DEEPWALK outperforms earlier methods in most cases (even before excluding their format-invalid outputs; see

13. Format-invalid “images” can still be saved as valid image files, because common image libraries truncate the pixel values into $[0, 255]$ before saving.

TABLE 6
Testing comprehensiveness (after excluding format-invalid images) achieved by different tools.

Criteria	Tool	ImageNet					CIFAR10				
		ResNet50	VGG16	MobileNet-V2	DenseNet121	Inception-V3	ResNet50	VGG16	MobileNet-V2	DenseNet121	Inception-V3
NC	Init.	59.73%	86.27%	88.15%	77.24%	82.60%	55.39%	41.75%	60.61%	61.94%	50.60%
	DEEPWALK	66.91%	88.75%	90.05%	82.37%	87.39%	64.37%	50.71%	64.01%	68.72%	54.39%
	DeepHunter	62.52%	82.45%	88.59%	78.61%	83.93%	60.62%	47.40%	61.26%	64.98%	51.37%
	TensorFuzz	60.10%	80.41%	88.21%	77.50%	83.12%	56.21%	42.58%	62.18%	62.16%	50.94%
	DeepSmart	60.65%	77.04%	88.40%	77.76%	83.00%	58.94%	45.98%	61.17%	62.98%	51.29%
	DeepTest	60.40%	76.39%	88.18%	77.31%	82.81%	56.89%	43.54%	60.69%	62.24%	50.77%
KMNC	Init.	0.59%	0.33%	0.58%	0.59%	0.59%	1.43	1.10	1.40	1.32	1.35
	DEEPWALK	3.04%	2.92%	3.11%	3.05%	2.88%	2.98%	2.83%	2.82%	2.95%	2.70%
	DeepHunter	1.93%	1.81%	3.32%	3.02%	2.63%	3.99%	2.50%	3.75%	2.22%	2.21%
	TensorFuzz	1.56%	1.75%	2.01%	1.99%	1.97%	1.52%	1.78%	1.79%	1.44%	1.39%
	DeepSmart	2.19%	1.82%	1.77%	2.13%	1.89%	2.74%	2.62%	2.78%	2.02%	1.63%
	DeepTest	0.79%	1.80%	1.52%	1.30%	1.39%	2.98%	2.58%	1.87%	2.38%	2.36%
SNAC	Init.	0	0	0	0	0	0	0	0	0	0
	DEEPWALK	2.63%	5.13%	3.18%	3.92%	7.72%	3.27%	7.44%	2.38%	3.31%	5.12%
	DeepHunter	0	0	0	0	0	0	0	0	0	0
	TensorFuzz	0	0	0	0	0	0	0	0	0	0
	DeepSmart	0	0	0	0	0	0	0	0	0	0
	DeepTest	0	0	0	0	0	0	0	0	0	0
NBC	Init.	0	0	0	0	0	0	0	0	0	0
	DEEPWALK	2.77%	5.22%	3.31%	3.89%	7.63%	5.99%	3.83%	2.84%	4.15%	5.79%
	DeepHunter	0	0	0	0	0	0	0	0	0	0
	TensorFuzz	0	0	0	0	0	0	0	0	0	0
	DeepSmart	0	0	0	0	0	0	0	0	0	0
	DeepTest	0	0	0	0	0	0	0	0	0	0
TKNC	Init.	52.25%	82.02%	70.12%	76.58%	87.23%	23.21%	23.24%	26.64%	57.46%	22.77%
	DEEPWALK	57.43%	86.92%	76.09%	81.32%	90.11%	26.24%	32.59%	28.13%	60.48%	25.43%
	DeepHunter	53.92%	83.77%	71.97%	78.01%	87.88%	24.43%	28.07%	27.25%	57.87%	22.58%
	TensorFuzz	52.50%	82.43%	70.97%	77.10%	87.30%	23.38%	23.77%	26.77%	57.63%	22.88%
	DeepSmart	53.06%	82.92%	71.56%	77.81%	87.50%	23.86%	26.38%	26.98%	57.61%	23.19%
	DeepTest	52.47%	82.23%	70.83%	76.79%	87.25%	23.55%	24.94%	26.77%	57.57%	22.96%

* "Init." denotes coverage achieved by seeds. Results are averaged over 5 runs with maximum standard deviation $< 10^{-3}$ (i.e., 0.0x%).

TABLE 7
Disclosed DNN faults (after excluding format-invalid images) using different tools.

Criteria	Tool	ImageNet					CIFAR10				
		ResNet-50	VGG16	MobileNet-V2	DenseNet121	Inception-V3	ResNet-50	VGG16	MobileNet-V2	DenseNet121	Inception-V3
NC	DEEPWALK	19679	9932	2591	3012	2287	4073	3044	799	1221	710
	DeepHunter	7455	5139	2531	2201	1196	2011	1714	631	630	419
	TensorFuzz	783	116	93	17	23	40	12	8	0	2
	DeepSmart	3963	2226	1118	939	1004	283	219	78	54	52
	DeepTest	614	662	102	132	171	697	690	162	202	279
	NLC	DEEPWALK	65387	86361	86226	53955	82313	21675	62765	35209	17233
DeepHunter		22311	11368	32691	11023	15692	7446	10043	9564	8789	9704
TensorFuzz		4979	4899	3128	4376	2287	1879	2876	2560	2340	1524
DeepSmart		29336	10676	33391	12201	13132	10196	22463	9917	8053	9177
DeepTest		4001	3367	5022	4189	4115	1007	886	1389	1053	1036
TFC		DEEPWALK	3209	7322	3063	3175	3330	1309	2128	882	771
	DeepHunter	1733	2871	993	901	1122	740	1395	563	364	601
	TensorFuzz	96	17	21	11	51	24	7	17	7	32
	DeepSmart	320	599	361	98	167	120	256	101	34	59
	DeepTest	1199	1310	433	307	511	411	504	212	301	371

Table 4). This shows that DEEPWALK’s mutations are better for exploring DNNs. In Fig. 9, we show how the coverage value in ResNet50 increases with NC on ImageNet and CIFAR10. DEEPWALK consistently achieves higher coverage during the testing process. Also, the coverage values tend to be stable; previous tools are unlikely to surpass DEEPWALK given more time budget. DeepTest terminates earlier than the other methods because it has exhausted all seeds: it discards a seed even if the seed increases coverage.

Interpretations. For KMNC in Table 6, DeepHunter performs better than DEEPWALK for three settings (i.e., ImageNet & MobileNet-V2, CIFAR10 & ResNet50, and CIFAR10 & MobileNet-V2). Recall Fig. 7 illustrates that existing tools explore an ε -radius sphere surrounding a seed. KMNC, in general, divides one neuron’s output range determined by the initial seeds into K -sections. Therefore, by intensively exploring the sphere near the seeds, DeepHunter can cover most sections checked by KMNC. However, for criteria that reflect the “corner-case” behavior of test inputs, such

as SNAC and NBC, all prior tools have zero increase. In contrast, DEEPWALK walks on the entire manifold (not just a sphere surrounding a seed), and it performs much better for SNAC and NBC. TKNC has similar coverage trending to that of NC because both focus on certain neurons with the highest outputs.

Low Coverage Increase. DEEPWALK exhibits relatively low increases on KMNC, SNAC, and NBC. DNN outputs were close to zero (similar to a normal distribution) due to input normalization and the presence of BN layers (which convert neuron outputs to zero-centered small values). Such small and normalized neuron outputs hardly reflect changes on these three fine-grained coverage criteria, particularly for SNAC and NBC which look for edge-case outputs. Also, model training datasets (e.g., ImageNet) are comprehensive. Therefore, most neuron output ranges are already covered when using the training data samples, which impedes testing tools to further increase coverage. As in Table 6, this is

TABLE 8
Ablation Results of DEEPWALK w/o \mathcal{T} .

	Comprehensiveness (%)					Faults (#)		
	NC	KMNC	SNAC	NBC	TKNC	NC	NLC	TFC
CIFAR10	60.94%	1.88%	0	0	24.50%	2265	11230	703
ImageNet	62.48%	1.95%	0	0	53.88%	7337	32134	1701

more obvious for DNNs having higher initial coverage (e.g., NC & ImageNet & MobileNet-V2).

Disclosed Faults. Table 7 lists the number of disclosed DNN faults when using different testing objectives. We only count an image as an error-triggering image if it is format valid. As introduced in Sec. 6, we use TFC and NLC, two non-structural coverage metrics, as the testing objectives when comparing the #faults disclosed by different tools. We also consider NC because it is one representative structural coverage. For all three objectives, DEEPWALK triggers the most faults for all DNNs, nearly doubling the amount of #faults found by DeepHunter in the majority of cases. When cross comparing DNNs trained on different datasets, we find that more faults are triggered for the ImageNet cases. This is reasonable, given that the large scale of ImageNet (1000 classes) makes the classification harder than that of CIFAR10 (10 classes). Moreover, we also note that when guided by NLC, all tools (including DEEPWALK) trigger more faults for all DNNs than the other two objectives. This result is consistent with observations in recent research as NLC can more accurately respond to DNN behaviors [19].

7.1.3 Ablation Study

To benchmark the “exploitation vs. exploration” strategy adopted by DEEPWALK (Sec. 5.3), we launch an ablation study to compare DEEPWALK with random walking (i.e., DEEPWALK w/o \mathcal{T}) on ResNet50. In line with the above evaluation, we conduct this ablation study across different coverage criteria. Results are presented in Table 8. Compared with Table 6 and Table 7, walking on manifolds to mutate perceptions, though randomly, is already comparable to DeepHunter (the best in the competitors). This illustrates that perceptual-level mutations can generally and effectively stress DNNs. Moreover, DEEPWALK (the ResNet50 columns in Table 6 and Table 7) notably outperforms random walking, showing the superiority of our walking strategy: it discovers useful perceptions and the desirable extent of changes from historical footprints.

7.2 Quality

We answer **RQ2** in Sec. 7.2. The quality of generated inputs is evaluated from the followings: ① recognizability, i.e., mutated images retain original labels, ② diversity of the triggered faults (as faults of higher diversity are more likely due to different root causes), and ③ usefulness of error-triggering inputs for repairing (i.e., model accuracy increases after retraining with error-triggering inputs). From the empirical perspective, we note that ① reflects the VAL of mutated images, and ② reflects the DIV of mutated (error-triggering) inputs. ③ reflects both DIV and VAL: the reason is that to increase the accuracy of the model, we demand the training data to be of high quality and diversity.

TABLE 9
Recognizability of mutated ImageNet images.

	DEEPWALK	DeepHunter	TensorFuzz	DeepSmart	DeepTest
IS	33.87±0.45	21.21±0.48	21.24±0.94	23.15±0.42	10.46±1.36
FID	54.31	70.13	75.09	67.06	119.89

7.2.1 Recognizability

Qualitative Comparison. Fig. 10 shows a comparison of mutated images. As DeepHunter limits the number of affine transformations applied on an image, its mutated images are similar to the original one. TensorFuzz limits the accumulated noise on one image within an L_∞ , retaining image perception. However, TensorFuzz generates outputs that are less diversified because its mutation patterns are limited. DeepSmart deconstructs images as it performs region-level mutations. DeepTest does not explicitly confine mutation operations. As in Fig. 10, it can apply affine transformations repeatedly on one image, resulting in an aberrant output. However, DEEPWALK mutates perceptions and produces diverse and perceptually meaningful outputs. Note that images mutated by DEEPWALK have relatively blurry backgrounds, as backgrounds are less associated with the perceptual constraints in manifolds. We present hundreds of DEEPWALK’s outputs for the reference at [1].

Quantitative Results. It’s challenging to manually exam the recognizability of mutated images given the large volumes. Humans may also disagree with the recognizability (see the “DeepTest” cases in Fig. 10). Two popular criteria, inception score (IS) [81] and Fréchet Inception Distance (FID) [82], are widely adopted in the AI community to assess recognizability of images by comparing them with known collections of real images. FID calculates distances from a *distribution* perspective and IS measures the similarity via a *class-aware* manner. IS/FID are suitable for our setting since we aim to check whether mutated images retrain their labels. In particular, we use them to measure how close the mutated images are towards the seeds. A smaller distance or higher similarity indicates that the mutated images are more recognizable and presumably retain the labels. The results are in Table 9. A higher IS is better, while a lower FID suggests more recognizability. Though earlier techniques launch input validations to keep realistic images, the images they regard as “realistic” manifest less recognizability than images mutated by DEEPWALK. Furthermore, we see these results as proof that, DEEPWALK, by addressing media data mutation and validation as a whole (via manifold), is much better for both input mutation and validation.

Mutations, not Memorization. DNNs are known for being able to memorize data points. To show that DEEPWALK indeed performs perceptual-level mutations rather than simply yields memorized training data, we calculate the similarity between the mutated images in Fig. 10 and each training image using SSIM [83], a popular image similarity metric. Fig. 11 shows the top-3 most similar training images regarding two mutated images. These training images still manifest distinct perceptions with DEEPWALK’s outputs, indicating that DEEPWALK constructs manifold to facilitate perceptual-level mutations, rather than mere memorization.



Fig. 10. Qualitative evaluation of existing tools and DEEPWALK.



Fig. 11. Mutated images and the most similar training data.

Mutated Perceptions. DEEPWALK forms perceptual transformations \mathcal{T} when walking on manifolds. Though manifolds have much lower dimensions (i.e., around 100), it is still hard to interpret which perceptions are primarily mutated by \mathcal{T} since several perceptions are jointly mutated. We observe that in most cases, perception mutations result in geometric-related changes, which is hardly achievable by prior approaches; see more visualizations in [1].

7.2.2 Diversity of Faults

Since different error-triggering inputs can be due to the same root cause, we measure the diversity of these DNN faults to quantify and compare the disclosed erroneous root causes: faults of higher diversity indicates more erroneous root causes are revealed in testing.

Erroneous Classes. Because all tested DNNs perform multi-label classification, we first count how many classes are covered by the disclosed faults. Results are given in Table 10. As noted, for ImageNet cases, DEEPWALK trigger DNN faults for most classes, which is around $3\times$ of the results of TensorFuzz. For CIFAR10 cases, faults triggered by DEEPWALK cover all classes. We interpret these results are highly promising: besides being effective to disclose more DNN faults, these faults also manifest a higher quality as they extensively reveal more diverse flaws.

Scaled Entropy. As reported in Table 10, since CIFAR10 only has 10 classes, most previous tool have triggered faults for all classes. Therefore, to further distinguish the diversity, we use scaled entropy as a metric. The scaled entropy is $-\frac{1}{|C|} \sum p_c \log p_c$, where $|C|$ is the number of classes and p_c is the proportion of outputs incorrectly predicted to be class c . Scaled entropy is in the range of $[0, 1]$, and a higher entropy suggests more diversity, i.e., less bias for particular classes. Table 10 shows that DEEPWALK outperforms others. We find that the scaled entropy is close to 1, indicating that findings of DEEPWALK are unbiased and almost evenly distributed across all classes for all three CIFAR10-DNNs.

7.2.3 Usefulness for Retraining

To “repair” DNNs, it’s common to retrain them using error-triggering inputs with ground truth labels [84], [85]. This

TABLE 10
Diversity of disclosed DNN faults.

	Tool	ImageNet ResNet-50	CIFAR10 ResNet-50	CIFAR10 VGG-16	CIFAR10 MobileNet-V2
#Class	DEEPWALK	849	10	10	10
	DeepHunter	691	10	10	10
	TensorFuzz	297	9	5	5
	DeepSmart	524	10	9	10
	DeepTest	306	10	9	7
Entropy ($\times 100$)	DEEPWALK	N/A	99.05	98.98	98.84
	DeepHunter	N/A	73.91	69.13	69.04
	TensorFuzz	N/A	N/A	N/A	N/A
	DeepSmart	N/A	94.76	N/A	91.29
	DeepTest	N/A	68.08	N/A	N/A

*The diversity evaluation is conducted in a two-step approach: 1) DNN faults are more diverse if the erroneous predictions cover more classes. 2) When the number of covered classes are equal, a higher entropy indicates more diverse DNN faults.

TABLE 11
Retraining accuracy (%) of ResNet50.

Init.	DEEPWALK	DeepHunter	TensorFuzz	DeepSmart	DeepTest
CIFAR10	94.07% \uparrow (All)	93.86% \uparrow	93.83% \uparrow	93.73% \downarrow	93.24% \downarrow
	93.77% 93.96% \uparrow (2K)	(All)	(All)	(All)	(All)
ImageNet	83.28% \uparrow (All)	78.86% \uparrow	78.32% \uparrow	72.90% \downarrow	72.16% \downarrow
	76.15% 80.75% \uparrow (7K)	(All)	(All)	(All)	(All)

*Results are averaged over 5 runs with maximum standard deviations $< 10^{-4}$.

process can be viewed as a way of performing data augmentation for the tested DNN [86], [87]. Table 11 shows the test accuracy after retraining of ResNet50 on CIFAR10 and ImageNet. For each tool, we take all of their discovered error-triggering inputs for retraining. Since DEEPWALK finds much more error-triggering inputs, to make the comparison fair (DeepHunter has 2,011 and 7,455 error-triggering inputs for CIFAR10 and ImageNet), we randomly selected 2K and 7K error-triggering inputs of DEEPWALK for retraining on CIFAR10 and ImageNet, respectively.

For both ImageNet and CIFAR10, DEEPWALK surpasses others in both settings, i.e., 83.28 (All) & 80.75 (7K) and 94.07 (All) & 93.96 (2K), indicating that the flaws detected by DEEPWALK are of high quality and diversity. It empirically reflects the VAL of perceptual-level mutations performed by DEEPWALK. We also emphasize that real-world DNNs may have been trained using standard data augmentation approaches like affine transformations [86]. Therefore, faults triggered by DEEPWALK are more desirable and orthogonal to those that may have been included in the augmented training data. It also explains why TensorFuzz retraining had the similar accuracy as DeepHunter, even though TensorFuzz triggered fewer faults.

Prior Tools Harm the Retraining. Retraining on datasets augmented by DeepSmart and DeepTest results in a decrease in accuracy. The region-wise mutation can break objects in images (see Fig. 10), and DeepTest may apply several affine modifications to an image, making it less recognizable. As a result, the mutated images may no longer

TABLE 12
Quantitative results of generalizability.

Task	Tool	Comprehensiveness	#Faults (NC)
Autonomous driving	DeepRoad	(+6.15, +0.58, +0.82)	2375
	DeepRoad _{rain}	(+7.36%, +16.14%, +2.32%)	2213
	DEEPWALK _{snow}	(+18.64%, +25.94%, +9.95%)	15547
Machine translation	DEEPWALK	+9.96%	4011
Audio classification	DEEPWALK	+4.04%	1449

retain the label and the follow-up retraining is therefore harmed. This evaluation shows the merit of manifold-based mutation; in comparison with other tools, Table 11 empirically illustrates that VAL (perceptual constraints) is retained by DEEPWALK, given that retraining on error-triggering inputs can notably enhance DNNs and outperform others.

Lower Improvements for Better DNNs. As a reported in Sec. 7.1, DNNs w.r.t. CIFAR10 are already well-trained to a saturating performance (i.e., the test accuracy no longer increases when trained with the original training data). Thus, an increased accuracy around 0.5% is indeed a big improvement — it is 5× of the improvement made by the best competitor (i.e., DeepHunter). In contrast, for the ResNet50 trained on ImageNet, since performing a 1000-class classification is more challenging, the initial accuracy is relatively lower. Accordingly, much higher improvements are made by retraining with error-triggering inputs of DEEPWALK (i.e., +7.13%); the gaps with improvements brought by other tools are also enlarged.

7.3 Generalizability

Settings. This section benchmarks the generalizability of DEEPWALK. Table 1 lists the models and datasets. The manifold of driving scenes has 512 dimensions and the text manifold has 100 dimensions. Since both these two datasets only have one class, we construct one manifold for each dataset. The audio dataset has 10 class; we construct 10 manifolds and the dimension is 128. Each of the experiment in this section runs for six hours.

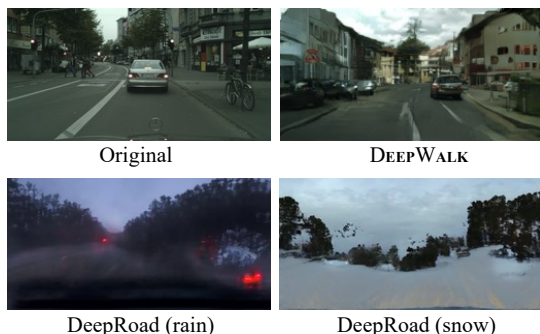


Fig. 12. (Mutated) driving scene images.

7.3.1 Autonomous Driving — Regression & Differential Testing

Differential Testing. Since the steering angle is likely to change when perceptions of a driving scene are mutated by DEEPWALK, we set up a differential testing scenario to form our oracle, in which steering angles predicted by three DNNs must match. The testing objective for this setting is the sum of values calculated on three target DNNs. The GAN model takes roughly one day for training due to

complexity of driving scenes. The tested DNNs are provided by DeepTest [3] with pre-trained parameters.

Comparison with DeepRoad. We compared DEEPWALK with DeepRoad. The mutated outputs are presented in Fig. 12. In addition to adjusting the road direction, DEEPWALK may also change the position/color of the car and background buildings, which introduces diverse driving scenes. We find that DeepRoad breaks original images when changing weathers. Therefore, its metamorphic oracle on steering angle consistency does *not* always hold. We also assess DeepRoad in the differential testing setting. In Table 12, we use NC to reflect the testing comprehensiveness and the number of faults are listed. DeepRoad uses additional data from other domains to deliver “style translation.” For instance, DeepRoad with a “rainy” scheme requires 1) seed driving scenes and 2) topologically similar scenes that offer rainy and sunny scenarios. Although DeepRoad is enhanced with additional knowledge, DEEPWALK outperforms it in both the testing comprehensiveness and #faults. Also, when NLC is used as the testing objective, 32,939 faults are triggered by DEEPWALK, which is more than twice of the #faults when using NC. This observation is consistent with our results in Sec. 7.1 — NLC is more effective to guide generating error-triggering inputs. Note that unlike other baseline tools, DeepRoad is not a feedback-driven tool; its triggered faults do not change with testing objectives.

It’s worth mentioning that, because the tested task is regression whose outputs are continuous, measuring the diversity of faults using entropy or #classes is infeasible. Nevertheless, since DEEPWALK comprehensively explores different perceptual-level mutations (e.g., mutating the background building or the car’s color; see more examples in [1]) and DNNs generally rely on perceptual properties in inputs to make predictions, it should be accurate to assume that faults triggered by DEEPWALK are due to more and different root causes. In addition, while analyzing root causes for DNN faults is still an open problem, we envision that perceptual-level mutations enabled by DEEPWALK can benefit future research for the interpretation and root cause analysis of DNN faults (see more discussions in Sec. 9).

Connection to Physical-World Attack/Testing. Previous works have conducted attacks/testings for autonomous driving systems via physical-world mutations [88], [89] (e.g., adding printable adversarial billboard [88]), which are more likely to occur in real world. Since manifolds in DEEPWALK are approximated in real-life images, we view the perceptual-level mutation in DEEPWALK as a potential direction for extending physical-world mutations. By approximating manifolds over real-life images, developers can observe which perceptual properties the autonomous driving system is sensitive to (i.e., the prediction can easily change when mutating these properties). These sensitive properties denote fault triggers that broadly exist in physical world and have more severe threats. With DEEPWALK, developers can repair the autonomous driving system in a more oriented manner.

7.3.2 Audio — More Complex Media Data

Settings. GAN for preparing manifold is built from stacked CNNs (see [1]) whose training completes in 2 hours. Audio clips of the same number being spoken lie in one manifold.

The target DNN was pre-trained with 93.96% test accuracy on the SC09 dataset. NC is used to reflect the testing comprehensiveness and results are given in Table 12.

Faults & Retraining. We note that a considerable number of faults are triggered. Overall, mutating audios is changing given the complex format. DEEPWALK directly mutates perceptions in audios which does not rely on any specific format and is very effective to trigger DNN faults. We further retrain the tested model on SC09 augmented with error-triggering inputs. The test accuracy improves to 94.52%, demonstrating the high quality of the mutated (error-triggering) audio recordings. The improvement is not high, which is reasonable because the tested DNN is already well-trained. Overall, we interpret the improvement in re-training as proving that DEEPWALK captures perceptual constraints on audios and produces realistic audios. We present mutated audios from all manifolds in [1].

7.3.3 Machine Translation — New Task & Discrete Data

Settings. DEEPWALK mutates natural language texts in a grammatically coherent manner, without prior knowledge or predefined templates [9], [10], [11]. The procedure is the same as mutating image or audio, except that we first use ARAE to encode discrete text into a continuous representation (discussed in Sec. 5.2). The whole training pipeline takes less than 2 hours. We use NC as the criteria. We test two jointly trained MT models, namely $E\vec{2}G$ and $G\vec{2}E$, that translate English (German) to German (English). Since MT primarily focuses on grammatical norms of languages, all English text can be viewed as being in one manifold.

<i>a child is walking away for nothing but candles.</i>
<i>a child walking to school in red.</i>
<i>the girl is studying away from her.</i>
<i>the children 's family is ready for their pictures.</i>

Fig. 13. Mutated sentences from the same seed.

Grammatical Coherence. DEEPWALK could build grammatically coherent yet different English sentences by walking on the constructed manifold. Empirically, we adopt the fluency score [90], [91] to assess coherence of mutated sentences. The fluency score, higher the better, ranges from [0, 1] and measures how fluent a sentence is via word dependencies. All mutated sentences achieve a fluency score of 0.32, suggesting strong coherence, compared to 0.35 for normal phrases in SNLI. We present several sample sentences in Fig. 13, which are mutated from the same seed. They are grammatically diverse and coherent, despite the fact that DEEPWALK does not specify or require templates to mutate texts. More examples of mutated sentences are shown in [1].

Back Translation. It’s generally hard to decide if MT makes translation errors. We form the testing oracle by assessing the consistency of $E\vec{2}G$ and $G\vec{2}E$. We convert an English sentence eng to a German sentence ger using $E\vec{2}G$ and then back to an English sentence eng' using $G\vec{2}E$; eng' should be highly similar with eng . An inconsistency indicates that at least one of the models translate incorrectly.

Testing Oracle & Results. We assess the similarity of eng and eng' via BLEU (Bi-Lingual Evaluation Under-

TABLE 13
Results of quantized DNN.

Quantized layer	Test acc. (%)	#Fault
Conv2D	58.37	139,122
Linear	58.32	146,793
Linear + Conv2D	58.32	165,065

study) [92]. The BLEU score is highly correlated with human assessment and ranges from [0, 1] (higher is better). We denote eng as an error-triggering input if the BLEU score between eng and eng' is 0. The sentence “A black dog carrying a metal to a man” is a fault-triggering sentence produced by DEEPWALK. This sentence is translated as “Ein schwarzer Hund hält einen Mann an” and is back-translated to “A black dog is holding a man”. Table 12 reports the testing comprehensiveness and #faults. DEEPWALK triggers a great number of faults in six hours. The results are encouraging, showing DEEPWALK’s adaptability in handling diverse media data types.

7.3.4 Quantized DNNs — A Black-Box Scenario

We also simulate a testing scenario for DNNs on mobile devices, where the DNN is quantized. We employ a MobileNet-V2 pretrained on ImageNet (officially shipped by PyTorch) and the quantization schemes are listed in Table 13. All three schemes quantize the layer parameters from 32-bit floating number to 8-bit integer. We present the test accuracy (on the randomly select 100 classes from ImageNet) in Table 13. The original model has 58.59% test accuracy, and the accuracy drops induced by quantization are negligible. The quantized models are thus deemed equivalent to the unquantized one. We use DEEPWALK to test these quantized models.

Black-Box Entropy. In this setting, applying white-/gray-box objectives is infeasible, since we only have the DNN output, i.e., a predicted label and the associate probability. We thus adopt the black-box entropy as the testing objective, which maximizes the difference of predicted probabilities from the DNN and the quantized one. Accordingly, we set up a differential testing oracle and denote a fault as an inconsistent prediction between the original and quantized DNN. The #faults are listed in Table 13. DEEPWALK produces a vast number of inconsistency-triggering inputs which reveal hidden defects introduced by quantization.

8 THREAT TO VALIDITY

Bias in Evaluations. Since this research compares DEEPWALK with prior tools, one threat is that the evaluation is biased. To mitigate this threat, we select a considerable number of DNNs that are widely studied in previous works [2], [3], [13], [93], [19], and commonly adopted as the backbone of modern deep learning systems. These 19 DNNs are representative in terms of tasks, structure, working scenarios, and featured platforms. We also consider five popular real-world datasets which consist of various data formats including image, audio, and text. In particular, the ImageNet dataset has been deemed as the “golden standard” of benchmarking DNNs for the past ten years. DNN testing objectives in our evaluation are also representative (e.g., structural, cluster-based, and distribution-aware) and proposed by research from both the AI and SE communities.

False Positives. Given that we report the faults disclosed by DEEPWALK, another threat is that there might be false positives, for instance, invalid inputs or mutated inputs whose ground truth labels are changed. We clarify that this issue should be eliminated from the following aspects. 1) Conceptually, data manifold aims to capture perceptual-level constraints of media data and DEEPWALK is based on manifolds provided by existing mature techniques. 2) Technically, manifolds are separately constructed for data of different labels and test inputs that are likely violate perceptual-level constraints (i.e., having high sensitivity; see Sec. 4) are pruned before testing. 3) Empirically, as evaluated in Sec. 7.1.1, DEEPWALK never generates format-invalid test inputs whereas prior tools frequently violates the format restriction of input. Also, Sec. 7.2.1 demonstrates that test inputs generated using DEEPWALK manifest the highest recognizability. Moreover, in Sec. 7.2.3, we retrain the tested DNNs: when using error-triggering inputs of DEEPWALK, the retrained DNNs have the highest improvements. Thus, it is reasonable to infer that false positives are largely eliminated in DEEPWALK’s results.

False Negatives. The third threat faced by DEEPWALK is that some DNN faults can be neglected. We clarify that, like all prior works in this field, DEEPWALK aims to test DNN rather than verify DNNs: it cannot guarantee to disclose all DNN faults. Nevertheless, we deem DEEPWALK as a powerful testing tool as it enables effective perceptual-level mutations and simultaneously retains the validity of mutated inputs. DEEPWALK manifests a high generalizability: it can test DNN of various 1) input formats (e.g., image and audio), 2) tasks (classification and regression), and 3) deployed scenarios/platforms (gray-box and black-box), under 4) different testing oracles (metamorphic and differential testing).

9 LIMITATIONS AND FUTURE WORKS

Fine-Grained Annotations. Perceptual-level mutations may break fine-grained annotations on DNN inputs. For instance, as shown in Sec. 7.3, when testing autonomous driving, the steering angle will be altered if the road in a driving scene is mutated via perceptual-level mutations. This threat can potentially harm the generalizability of perceptual-level mutations for (metamorphic) testing of DNNs under certain scenarios. Nevertheless, this issue is not specifically induced by DEEPWALK; geometrical mutations (since steering angle is tied to geometrical properties) and the knowledge transfer in DeepRoad (see examples in Fig. 12) can also change the ground truth steering angle in the mutated images.

On the other hand, for previous tools performing mutation on data bytes (e.g., pixel-level mutations), although they may produce invalid and unnatural data, they can reuse the dense annotation in most cases if the operator and validator are carefully designed by human experts.

Recall as we show in Fig. 7, previous mutations explore the ϵ -radius sphere around the original input. Thus, to alleviate the above threat, it is possible to retain the human annotations by restricting the footsteps when DEEPWALK is walking on manifold—with the diversity of mutation is unavoidably sacrificed. In addition, users may construct “sub-manifolds” within one manifold, for instance, given a collection of driving scenes, users can construct a “sub-

manifold” that corresponds to driving scenes of directing-to-left road. We leave these as future works.

Testing Objective. Most testing objectives aim to capture the behaviors/states of DNNs [2], [69], [19]. Nonetheless, understanding internal mechanisms of DNNs is still an open problem, which impedes further developments of DNN coverage. Since DNNs make prediction based on perceptual properties in inputs, we view proposing perception coverage metrics as a promising research direction. That is, instead of counting states of DNNs, we can count how many perceptual properties are covered during testing. Unlike existing coverage metrics which may depend on how tested DNNs are implemented, perception coverage is agnostic to the implementations of DNNs, because it is defined in the input space. In addition, perception coverage is orthogonal to existing coverage metrics that focus on DNN behaviors. In that sense, it can be combined with existing coverage metrics to form a hybrid coverage to better characterize the testing comprehensiveness.

Testing Oracle. Existing works mainly define testing oracles for DNN outputs, i.e., whether the DNN (or multiple DNNs) have consistent predictions before/after mutations. One recent work advocates to define oracle over the decision process of DNNs [93] (i.e., decision oracle). Despite viewing from different angles, they do not distinguish DNN faults. Therefore, we deem forming perceptual-level oracle as an interesting future direction. More concretely, the oracle checks whether the DNN makes consistent prediction before/after mutating certain perceptual properties. Compared with existing oracles, perceptual-level oracles are more fine-grained, as it separates DNN faults according to the mutated perceptual properties. Moreover, perceptual-level oracles are orthogonal to existing output- and decision-based oracles; perceptual-level oracles can also be combined with prior oracles to form hybrid ones and reflect DNN faults in a faith manner.

Interpretable Root Cause Analysis. We view employing DEEPWALK for interpretable root cause analysis of DNNs as a highly feasible research direction. Compared with previous mutations (e.g., adding noise), perceptual-level mutations enabled by DEEPWALK are more understandable and interpretable for human developers. For instance, when a DNN fault is triggered after mutating the ear in a dog photo, the developer can conclude that the DNN focuses on ears to recognize dogs and accordingly fix this bias. Moreover, since DEEPWALK maintains \mathcal{T} to record its footsteps on data manifolds, by visualizing mutations depicted by \mathcal{T} , developers can holistically decide which perceptual properties the DNN is most vulnerable to.

10 CONCLUSION

This research formulates the key objectives in mutating DNN inputs, DIV and VAL. We prove that DIV and VAL inextricably bounds each other, and rebut SOTA works on their applicability of mutating real-world media data. We then present DEEPWALK for mutating media data to achieve high DIV and VAL with provably guarantee. Our evaluation shows DEEPWALK’s high effectiveness, exceeding prior works in both general image classification and domain-specific scenarios.

REFERENCES

- [1] Artifact, "Deepwalk," Anonymized link, 2022.
- [2] K. Pei, Y. Cao, J. Yang, and S. Jana, "DeepXplore: Automated whitebox testing of deep learning systems," in *Proceedings of the 26th Symposium on Operating Systems Principles*, ser. SOSP '17. New York, NY, USA: ACM, 2017, pp. 1–18. [Online]. Available: <http://doi.acm.org/10.1145/3132747.3132785>
- [3] Y. Tian, K. Pei, S. Jana, and B. Ray, "DeepTest: Automated testing of deep-neural-network-driven autonomous cars," ser. ICSE '18, 2018.
- [4] M. Zhang, Y. Zhang, L. Zhang, C. Liu, and S. Khurshid, "DeepRoad: GAN-based Metamorphic Testing and Input Validation Framework for Autonomous Driving Systems," in *ASE*, 2018.
- [5] A. Odena and I. Goodfellow, "Tensorfuzz: Debugging neural networks with coverage-guided fuzzing," *arXiv preprint arXiv:1807.10875*, 2018.
- [6] J. Wang, G. Dong, J. Sun, X. Wang, and P. Zhang, "Adversarial sample detection for deep neural network through model mutation testing," ser. ICSE, 2019.
- [7] A. Dwarakanath, M. Ahuja, S. Sikand, R. M. Rao, R. P. J. C. Bose, N. Dubash, and S. Podder, "Identifying implementation bugs in machine learning based image classifiers using metamorphic testing," in *ISSTA*, 2018.
- [8] S. Nakajima and T. Y. Chen, "Generating biased dataset for metamorphic testing of machine learning programs," in *IFIP-ICTSS*, 2019.
- [9] S. Galhotra, Y. Brun, and A. Meliou, "Fairness testing: testing software for discrimination," in *ACM ESEC/FSE*. ACM, 2017, pp. 498–510.
- [10] S. Udeshi, P. Arora, and S. Chattopadhyay, "Automated directed fairness testing," ser. ASE, 2018.
- [11] P. Ma, S. Wang, and J. Liu, "Metamorphic testing and certified mitigation of fairness violations in nlp models," in *IJCAI*, 2020, pp. 458–465.
- [12] P. He, C. Meister, and Z. Su, "Structure-invariant testing for machine translation," in *ICSE*, 2020.
- [13] X. Xie, L. Ma, F. Juefei-Xu, H. Chen, M. Xue, B. Li, Y. Liu, J. Zhao, J. Yin, and S. See, "Coverage-guided fuzzing for deep neural networks," *arXiv preprint arXiv:1809.01266*, 2018.
- [14] S. Kang, R. Feldt, and S. Yoo, "Sinvad: Search-based image space navigation for dnn image classifier test input generation," in *Proceedings of the IEEE/ACM 42nd International Conference on Software Engineering Workshops*, 2020, pp. 521–528.
- [15] S. Dola, M. B. Dwyer, and M. L. Soffa, "Distribution-aware testing of neural networks using generative models," in *2021 IEEE/ACM 43rd International Conference on Software Engineering (ICSE)*. IEEE, 2021, pp. 226–237.
- [16] L. Deng, "The mnist database of handwritten digit images for machine learning research [best of the web]," *IEEE Signal Processing Magazine*, vol. 29, no. 6, pp. 141–142, 2012.
- [17] Y. Bengio, A. Courville, and P. Vincent, "Representation learning: A review and new perspectives," *IEEE transactions on pattern analysis and machine intelligence*, vol. 35, no. 8, pp. 1798–1828, 2013.
- [18] B. Zhu, J. Z. Liu, S. F. Cauley, B. R. Rosen, and M. S. Rosen, "Image reconstruction by domain-transform manifold learning," *Nature*, vol. 555, no. 7697, pp. 487–492, 2018.
- [19] Y. Yuan, Q. Pang, and S. Wang, "Revisiting neuron coverage for dnn testing: A layer-wise and distribution-aware criterion," in *45th IEEE/ACM International Conference on Software Engineering (ICSE)*, 2023.
- [20] S. Demird, H. F. Eniser, and A. Sen, "DeepSmartFuzzer: Reward guided test generation for deep learning," *arXiv preprint arXiv:1911.10621*, 2019.
- [21] Y. LeCun, F. J. Huang, and L. Bottou, "Learning methods for generic object recognition with invariance to pose and lighting," in *Proceedings of the 2004 IEEE Computer Society Conference on Computer Vision and Pattern Recognition*, 2004. CVPR 2004., vol. 2. IEEE, 2004, pp. II–104.
- [22] T. Mikolov, M. Karafiát, L. Burget, J. Černocký, and S. Khudanpur, "Recurrent neural network based language model," in *Eleventh annual conference of the international speech communication association*, 2010.
- [23] J. A. Lee and M. Verleysen, *Nonlinear dimensionality reduction*. Springer Science & Business Media, 2007.
- [24] X. Fan, W. Jiang, H. Luo, and M. Fei, "Spherereid: Deep hypersphere manifold embedding for person re-identification," *Journal of Visual Communication and Image Representation*, vol. 60, pp. 51–58, 2019.
- [25] H. Abdi and L. J. Williams, "Principal component analysis," *Wiley interdisciplinary reviews: computational statistics*, vol. 2, no. 4, pp. 433–459, 2010.
- [26] M. Balasubramanian, E. L. Schwartz, J. B. Tenenbaum, V. de Silva, and J. C. Langford, "The ISOMAP algorithm and topological stability," *Science*, vol. 295, no. 5552, pp. 7–7, 2002.
- [27] S. T. Roweis and L. K. Saul, "Nonlinear dimensionality reduction by locally linear embedding," *science*, vol. 290, no. 5500, pp. 2323–2326, 2000.
- [28] M. Belkin and P. Niyogi, "Laplacian eigenmaps for dimensionality reduction and data representation," *Neural computation*, vol. 15, no. 6, pp. 1373–1396, 2003.
- [29] J.-Y. Zhu, P. Krähenbühl, E. Shechtman, and A. A. Efros, "Generative visual manipulation on the natural image manifold," in *European conference on computer vision*. Springer, 2016, pp. 597–613.
- [30] D. Cai and X. He, "Manifold adaptive experimental design for text categorization," *IEEE Transactions on Knowledge and Data Engineering*, vol. 24, no. 4, pp. 707–719, 2011.
- [31] H. Guo, "Nonlinear mixup: Out-of-manifold data augmentation for text classification," in *Proceedings of the AAAI Conference on Artificial Intelligence*, vol. 34, no. 04, 2020, pp. 4044–4051.
- [32] H. Li, B. Baucom, and P. Georgiou, "Unsupervised latent behavior manifold learning from acoustic features: Audio2behavior," in *2017 IEEE international conference on acoustics, speech and signal processing (ICASSP)*. IEEE, 2017, pp. 5620–5624.
- [33] F. Briggs, R. Raich, and X. Z. Fern, "Audio classification of bird species: A statistical manifold approach," in *2009 Ninth IEEE international conference on data mining*. IEEE, 2009, pp. 51–60.
- [34] Z. Li, M. Pan, T. Zhang, and X. Li, "Testing dnn-based autonomous driving systems under critical environmental conditions," in *Proceedings of the 38th International Conference on Machine Learning*, ser. Proceedings of Machine Learning Research, M. Meila and T. Zhang, Eds., vol. 139. PMLR, 18–24 Jul 2021, pp. 6471–6482.
- [35] J.-Y. Zhu, T. Park, P. Isola, and A. A. Efros, "Unpaired image-to-image translation using cycle-consistent adversarial networks," in *Proceedings of the IEEE international conference on computer vision*, 2017, pp. 2223–2232.
- [36] M.-Y. Liu, T. Breuel, and J. Kautz, "Unsupervised image-to-image translation networks," in *Advances in neural information processing systems*, 2017, pp. 700–708.
- [37] J.-Y. Zhu, "CycleGAN Failure Cases," <http://github.com/junyanz/CycleGAN#failure-cases>, 2021.
- [38] K. Simonyan and A. Zisserman, "Very deep convolutional networks for large-scale image recognition," *arXiv preprint arXiv:1409.1556*, 2014.
- [39] T. Byun, A. Vijayakumar, S. Rayadurgam, and D. Cofer, "Manifold-based test generation for image classifiers," in *2020 IEEE International Conference On Artificial Intelligence Testing (AITest)*. IEEE, 2020, pp. 15–22.
- [40] T. Byun and S. Rayadurgam, "Manifold for machine learning assurance," in *2020 IEEE/ACM 42nd International Conference on Software Engineering: New Ideas and Emerging Results (ICSE-NIER)*. IEEE, 2020, pp. 97–100.
- [41] G. Han, Z. Li, Y. Wei, C. Hu, S. Guo, Y. Zhang, X.-S. Xu, and T. Peng, "FuzzGAN: A generation-based fuzzing framework for testing deep neural networks," <https://g3h4n.github.io/publication/FuzzGAN>, 2019.
- [42] I. Goodfellow, J. Pouget-Abadie, M. Mirza, B. Xu, D. Warde-Farley, S. Ozair, A. Courville, and Y. Bengio, "Generative adversarial nets," in *Advances in neural information processing systems*, 2014, pp. 2672–2680.
- [43] D. P. Kingma and M. Welling, "Auto-encoding variational bayes," in *Advances in Neural Information Processing Systems*, 2014.
- [44] J. Deng, W. Dong, R. Socher, L.-J. Li, K. Li, and L. Fei-Fei, "ImageNet: A Large-Scale Hierarchical Image Database," in *CVPR09*, 2009.
- [45] S. Ross, *A first course in probability*. Pearson, 2010.
- [46] G. Bratski and A. Kaehler, "Opencv," *Dr. Dobb's journal of software tools*, vol. 3, p. 2, 2000.
- [47] M. Arjovsky, S. Chintala, and L. Bottou, "Wasserstein generative adversarial networks," in *International conference on machine learning*. PMLR, 2017, pp. 214–223.

- [48] T. Miyato, T. Kataoka, M. Koyama, and Y. Yoshida, "Spectral normalization for generative adversarial networks," in *International Conference on Learning Representations*, 2018.
- [49] H. Zhang, I. Goodfellow, D. Metaxas, and A. Odena, "Self-attention generative adversarial networks," in *International conference on machine learning*. PMLR, 2019, pp. 7354–7363.
- [50] A. Brock, J. Donahue, and K. Simonyan, "Large scale gan training for high fidelity natural image synthesis," in *International Conference on Learning Representations*, 2018.
- [51] M. S. Sajjadi, O. Bachem, M. Lucic, O. Bousquet, and S. Gelly, "Assessing generative models via precision and recall," *Advances in Neural Information Processing Systems*, vol. 31, 2018.
- [52] U. Tanielian, T. Issenuth, E. Dohmatob, and J. Mary, "Learning disconnected manifolds: a no gan's land," in *International Conference on Machine Learning*. PMLR, 2020, pp. 9418–9427.
- [53] R. Novak, Y. Bahri, D. A. Abolafia, J. Pennington, and J. Sohl-Dickstein, "Sensitivity and generalization in neural networks: an empirical study," in *International Conference on Learning Representations*, 2018.
- [54] D. Holden, J. Saito, T. Komura, and T. Joyce, "Learning motion manifolds with convolutional autoencoders," in *SIGGRAPH Asia 2015 Technical Briefs*, 2015, pp. 1–4.
- [55] F. J. Martinez-Murcia, A. Ortiz, J.-M. Gorriz, J. Ramirez, and D. Castillo-Barnes, "Studying the manifold structure of alzheimer's disease: A deep learning approach using convolutional autoencoders," *IEEE journal of biomedical and health informatics*, vol. 24, no. 1, pp. 17–26, 2019.
- [56] Y. Saito, S. Takamichi, and H. Saruwatari, "Statistical parametric speech synthesis incorporating generative adversarial networks," *IEEE/ACM Transactions on Audio, Speech, and Language Processing*, vol. 26, no. 1, pp. 84–96, 2017.
- [57] D. P. Kingma and P. Dhariwal, "Glow: Generative flow with invertible 1x1 convolutions," *Advances in neural information processing systems*, vol. 31, 2018.
- [58] J. Ho, A. Jain, and P. Abbeel, "Denoising diffusion probabilistic models," *NeurIPS*, vol. 33, pp. 6840–6851, 2020.
- [59] "Stable diffusion online," <https://stablediffusionweb.com/>, 2023.
- [60] J. Zhao, Y. Kim, K. Zhang, A. Rush, and Y. LeCun, "Adversarially regularized autoencoders," in *ICML*. PMLR, 2018.
- [61] A. Radford, L. Metz, and S. Chintala, "Unsupervised representation learning with deep convolutional generative adversarial networks," *arXiv preprint arXiv:1511.06434*, 2015.
- [62] S. Ioffe and C. Szegedy, "Batch normalization: Accelerating deep network training by reducing internal covariate shift," in *ICML*. PMLR, 2015, pp. 448–456.
- [63] H. De Vries, F. Strub, J. Mary, H. Larochelle, O. Pietquin, and A. Courville, "Modulating early visual processing by language," *arXiv preprint arXiv:1707.00683*, 2017.
- [64] S. Ruder, "An overview of gradient descent optimization algorithms," *arXiv preprint arXiv:1609.04747*, 2016.
- [65] D. P. Kingma and J. Ba, "Adam: A method for stochastic optimization," 2014.
- [66] C. J. Watkins and P. Dayan, "Q-learning," *Machine learning*, vol. 8, no. 3-4, pp. 279–292, 1992.
- [67] A. Danial, "CLOC," <https://github.com/AIDanial/cloc>, 2017.
- [68] "Optimized implementations of DNN coverage metrics," <https://github.com/Yuanyuan-Yuan/Neural-Coverage>, 2023.
- [69] L. Ma, F. Juefei-Xu, J. Sun, C. Chen, T. Su, F. Zhang, M. Xue, B. Li, L. Li, Y. Liu *et al.*, "DeepGauge: Comprehensive and multi-granularity testing criteria for gauging the robustness of deep learning systems," in *Proceedings of the 33rd ACM/IEEE International Conference on Automated Software Engineering*, ser. ASE 2018, 2018.
- [70] K. He, X. Zhang, S. Ren, and J. Sun, "Deep residual learning for image recognition," in *Proceedings of the IEEE conference on computer vision and pattern recognition*, 2016.
- [71] A. G. Howard, M. Zhu, B. Chen, D. Kalenichenko, W. Wang, T. Weyand, M. Andreetto, and H. Adam, "Mobilenets: Efficient convolutional neural networks for mobile vision applications," *arXiv preprint arXiv:1704.04861*, 2017.
- [72] C. Szegedy, V. Vanhoucke, S. Ioffe, J. Shlens, and Z. Wojna, "Rethinking the inception architecture for computer vision," in *Proceedings of the IEEE conference on computer vision and pattern recognition*, 2016, pp. 2818–2826.
- [73] G. Huang, Z. Liu, L. Van Der Maaten, and K. Q. Weinberger, "Densely connected convolutional networks," in *Proceedings of the IEEE conference on computer vision and pattern recognition*, 2017, pp. 4700–4708.
- [74] A. Vaswani, N. Shazeer, N. Parmar, J. Uszkoreit, L. Jones, A. N. Gomez, L. Kaiser, and I. Polosukhin, "Attention is all you need," *arXiv preprint arXiv:1706.03762*, 2017.
- [75] Y. Yuan, Q. Pang, and S. Wang, "Automated side channel analysis of media software with manifold learning," in *31st USENIX Security Symposium (USENIX Security 22)*, 2022, pp. 4419–4436.
- [76] A. Krizhevsky, G. Hinton *et al.*, "Learning multiple layers of features from tiny images," 2009.
- [77] J. Deng, W. Dong, R. Socher, L.-J. Li, K. Li, and L. Fei-Fei, "Imagenet: A large-scale hierarchical image database," in *2009 IEEE conference on computer vision and pattern recognition*. Ieee, 2009, pp. 248–255.
- [78] M. Cordts, M. Omran, S. Ramos, T. Rehfeld, M. Enzweiler, R. Benenson, U. Franke, S. Roth, and B. Schiele, "The cityscapes dataset for semantic urban scene understanding," in *Proceedings of the IEEE conference on computer vision and pattern recognition*, 2016, pp. 3213–3223.
- [79] S. Bowman, G. Angeli, C. Potts, and C. D. Manning, "A large annotated corpus for learning natural language inference," in *Proceedings of the 2015 Conference on Empirical Methods in Natural Language Processing*, 2015, pp. 632–642.
- [80] C. Donahue, J. McAuley, and M. Puckette, "Adversarial audio synthesis," in *International Conference on Learning Representations*, 2019.
- [81] T. Salimans, I. Goodfellow, W. Zaremba, V. Cheung, A. Radford, and X. Chen, "Improved techniques for training gans," *Advances in neural information processing systems*, vol. 29, pp. 2234–2242, 2016.
- [82] M. Heusel, H. Ramsauer, T. Unterthiner, B. Nessler, and S. Hochreiter, "Gans trained by a two time-scale update rule converge to a local nash equilibrium," in *Advances in neural information processing systems*, 2017, pp. 6626–6637.
- [83] Z. Wang, A. C. Bovik, H. R. Sheikh, and E. P. Simoncelli, "Image quality assessment: from error visibility to structural similarity," *IEEE transactions on image processing*, vol. 13, no. 4, pp. 600–612, 2004.
- [84] S. Wang and Z. Su, "Metamorphic object insertion for testing object detection systems," in *ASE*, 2020.
- [85] X. Zhang, J. Zhai, S. Ma, and C. Shen, "Autotrainer: An automatic dnn training problem detection and repair system," in *2021 IEEE/ACM 43rd International Conference on Software Engineering (ICSE)*, 2021, pp. 359–371.
- [86] C. Shorten and T. M. Khoshgoftaar, "A survey on image data augmentation for deep learning," *Journal of Big Data*, vol. 6, no. 1, pp. 1–48, 2019.
- [87] S. Yun, D. Han, S. J. Oh, S. Chun, J. Choe, and Y. Yoo, "Cutmix: Regularization strategy to train strong classifiers with localizable features," in *Proceedings of the IEEE/CVF international conference on computer vision*, 2019, pp. 6023–6032.
- [88] H. Zhou, W. Li, Z. Kong, J. Guo, Y. Zhang, B. Yu, L. Zhang, and C. Liu, "Deepbillboard: Systematic physical-world testing of autonomous driving systems," in *Proceedings of the ACM/IEEE 42nd International Conference on Software Engineering*, 2020, pp. 347–358.
- [89] T. Sato, J. Shen, N. Wang, Y. Jia, X. Lin, and Q. A. Chen, "Dirty road can attack: Security of deep learning based automated lane centering under physical-world attack," in *Proceedings of the 30th USENIX Security Symposium (USENIX Security 21)*, 2021.
- [90] T. Ge, F. Wei, and M. Zhou, "Fluency boost learning and inference for neural grammatical error correction," in *Proceedings of the 56th Annual Meeting of the Association for Computational Linguistics (Volume 1: Long Papers)*, 2018, pp. 1055–1065.
- [91] P. Ma and S. Wang, "Mt-teql: Evaluating and augmenting consistency of text-to-sql models with metamorphic testing," *arXiv preprint arXiv:2012.11163*, 2020.
- [92] K. Papineni, S. Roukos, T. Ward, and W.-J. Zhu, "Bleu: a method for automatic evaluation of machine translation," in *Proceedings of the 40th annual meeting of the Association for Computational Linguistics*, 2002, pp. 311–318.
- [93] Y. Yuan, Q. Pang, and S. Wang, "Unveiling hidden dnn defects with decision-based metamorphic testing," in *37th IEEE/ACM International Conference on Automated Software Engineering*, 2022, pp. 1–13.